2016

Dynamic Response of Aerospace Materials Subjected to Extreme Environments

Craig Tilton
University of Rhode Island, craig_tilton@my.uri.edu

DYNAMIC RESPONSE OF AEROSPACE MATERIALS SUBJECTED TO EXTREME ENVIRONMENTS

BY

CRAIG TILTON

A THESIS SUBMITTED IN PARTIAL FULFILLMENT OF THE

REQUIREMENTS FOR THE DEGREE OF

MASTER OF SCIENCE

IN

MECHANICAL ENGINEERING AND APPLIED MECHANICS

UNIVERSITY OF RHODE ISLAND

2016

MASTER OF SCIENCE THESIS

OF

CRAIG TILTON

APPROVED:

Thesis Committee:

Major Professor Arun Shukla

DML Meyer

George Tsiatas

Nasser H. Zawia
DEAN OF THE GRADUATE SCHOOL

UNIVERSITY OF RHODE ISLAND
2016

ABSTRACT

An experimental investigation was conducted subjecting Hastelloy X plates to shock loadings. The study seeks to understand the structural response of these aerospace materials when subjected to a combination of high temperature and shock loading with different boundary conditions.

First, an exhaustive series of experiments was conducted simultaneously subjecting Hastelloy X plates to extreme temperatures, in-plane tensile loading, and transverse shock loading. To achieve these loadings, a shock tube apparatus was used in conjunction with a novel hydraulic pre-loading fixture outfitted with propane flame torches. Experiments were carried out at peak shock loads of 1.7 and 3.1 MPa, temperatures up to 900ºC, and in-plane tensile loads up to 80% of the yield strength of the material at the given temperature. High speed photography and Digital Image Correlation (DIC) was used to obtain full-field, three-dimensional deformation information during the event. It is evident that the addition of a tensile pre-load reduces the maximum deflection for all temperatures. However, further increasing the magnitude of a pre-existing tensile pre-load has diminishing returns at temperatures above 400 ºC. It was seen that the specimen experiences a decrease in resistance to deformation caused by a blast loading for temperatures until 800°C. However, at 900°C, the specimen's resistance was observed to be greater than at 800°C. It was also observed that an indentation mode of deformation occurs at high temperatures in the case of 3.1 MPa peak load case but for no temperature in the 1.7 MPa peak load case.

Next, a comprehensive series of experiments was conducted subjecting cantilevered Hastelloy X plates to extreme temperatures and oblique shock loadings. A shock tube was used to achieve consistent planar shock waves and was supplemented by four propane torches to obtain high specimen temperatures. To capture the deformation event, high speed photography was used in conjunction with DIC to attain full-field, three-dimensional deflections, velocities, and strains. Experiments were conducted at temperatures of 25°C, 400°C, and 800°C and shock angles of 0° (normal), 15°, and 30°. It is evident that an increase in temperature causes an increased magnitude in out-of-plane deflection and in certain cases causes the deformations to occur in mode II. It is also observed that increasing the angle of the specimen relative to the shock decreases the magnitude of out-of-plane deformation.

ACKNOWLEDGMENTS

First and foremost, I would like to sincerely thank my advisor Dr. Shukla. Dr. Shukla invited me to work in his lab in 2013 while I was an undergraduate and has since served as an inspiration and mentor. He has elevated my work and character to new heights I had never dreamed of and is the main reason I have become so passionate about research. I feel honored to have worked in such a wonderful lab that continues to do incredible things. Thank you Dr. Shukla for your wisdom and guidance during my three fantastic years in the DPML.

I would also like to thank Dr. Tsiatas and Dr. Meyer for being members of my committee. In addition to being a member of my committee, I would like to thank Dr. Meyer for her commitment to her students which has served as an inspiration throughout my years at URI.

I would like to acknowledge my friends in the lab: Sandeep Abotula, Dan Clarkin, Laura Corvese, Nick Denardo, Payam Fahr, Mark Farat, Erin Gauch, Sachin Gupta, Nick Heeder, Carlos Javier, Shyamal Kishore, Nathan Kross, Frank Livolsi, Emad Makki, Helio Matos, Kim McCarthy, Prathmesh Parrikar, Tyler Patten, Mike Pinto, Dom Safina, Chris Salazar, Chris Shillings, and Jefferson Wright who have made this experience all the more enjoyable. I would also like to thank the MCISE department especially AJ Bothun, Jim Byrnes, Jen Cerullo, Rob D'Ambrosca, Nancy Dubee, Dave Ferriera, Joe Gomez, Sally Marinelli, and Donna Mattera.

I would like to thank the financial support of the Air Force Office of Scientific Research (AFOSR) under Grant No. FA9550-13-1-0037.

Last but certainly not least, I would like to express my gratitude to my parents, Carol and Ken, and my sisters, Christine and Sydney, for their unconditional support and love. I also want to thank all of my extended family in Florida and Newfoundland. I wouldn't be where I am today without the support of my family and friends.

PREFACE

An experimental study was conducted exploring the dynamic mechanisms of deformation of Hastelloy X. In aerospace applications, it is imperative that the materials used in structures are well understood in extreme combinations of conditions. Therefore, this work seeks to provide otherwise unavailable, critical information to the Air Force in order to design structures essential to our nations well-being. This thesis is prepared using the manuscript format.

Chapter 1 details the experiments conducted on Hastelloy X plates simultaneously subjected to extreme temperatures, in-plane tensile loads, and transverse shock loads. This work evaluates the structural response of thin plates using high speed photography and Digital Image Correlation. Here, the relationship between deformation, temperature, shock load, and in-plane load is discussed. This chapter follows the formatting guidelines specified by *Experimental Mechanics*.

Chapter 2 outlines the experiments conducted subjecting cantilevered Hastelloy X plates to extreme temperatures and oblique shock loading. This work investigates the structural response of these plates with respect to temperature and angle of the impinging shock. This chapter follows the formatting guidelines specified by *The Journal of Impact Engineering*.

TABLE OF CONTENTS

ABSTRACT ii

ACKNOWLEDGMENTS iv

PREFACE vi

TABLE OF CONTENTS vii

LIST OF TABLES ix

LIST OF FIGURES x

CHAPTER 1 1

Abstract 2

Introduction 3

Experimental Procedures 5

Material and Specimen Geometry 5
Pre-Load Apparatus 5
High Temperature 7
Shock Tube 8

Results and Discussion 12

A. Shock pressure: 1.7 MPa, pre-load: no pre-load. 12
B. Incident pressure: 1.7 MPa, pre-load: 50% yield. 17
C. Incident pressure: 1.7 MPa, pre-load: 80% yield. 18
D. Incident pressure: 1.7 MPa, all loads 19
E. Incident pressure: 3.1 MPa, pre-load: no pre-load. 21
F. Incident pressure: 3.1 MPa, pre-load: 80% yield. 24
G. Incident pressure: 3.1 MPa, all loads. 26

Conclusions 30

Acknowledgements 31

References 32

CHAPTER 2 35

Abstract 36

Introduction 37

Experimental Procedures 39

Material and Specimen Geometry 39

High Temperature 40

Shock Tube 41

High Speed Photography and Digital Image Correlation 43

Results and Discussion 44

Conclusions 53

Acknowledgements 55

References 56

Conclusions & Future Work 58

LIST OF TABLES

Table 1: This table displays whether or not indentation occurred with a “Y” indicating that indentation did occur……27

LIST OF FIGURES

CHAPTER 1

Figure 1: Novel tensile pre-load apparatus developed for these experiments. 7

Figure 2: (a) Thermocouple locations (b) Typical temperature distribution..... 8

Figure 3: Shock tube apparatus and muzzle (a) actual (b) schematic. 9

Figure 4: (a) 1.7 MPa pressure profile (b) 3.1 MPa pressure profile. 10

Figure 5: Camera locations for digital image correlation and side view. 11

Figure 6: Side view images of a room temperature, no pre-load experiment. The numbers indicate the time in ms from when the incident pulse triggered the cameras. 13

Figure 7: Out-of-plane deflection contours from DIC for a room temperature, no pre-load experiment. 14

Figure 8: Center point, out-of-plane deflection for the 1.7 MPa, no pre-load series... 15

Figure 9: (a) Yield strength as a function of temperature for Hastelloy X where the solid, blue curve is a quasi-static strain rate [24] while the dashed, red curve is a high strain rate (5000/s) [22]. (b) Dynamic modulus of elasticity as a function of temperature for Hastelloy X [3]. 16

Figure 10: Center point, out-of-plane deflection for the 1.7 MPa, 50% yield pre-load series. 18

Figure 11: Center point, out-of-plane deflection for the 1.7 MPa, 80% yield series... 19

Figure 12: The maximum, center point, out-of-plane deflection as a function of temperature for the three pre-load scenarios. 20

Figure 13: Out-of-plane deflection contours from DIC for an 800°C, no pre-load experiment. 21
Figure 14: Center point, out-of-plane velocity for the 3.1 MPa, no pre-load series. ... 23
Figure 15: Center point, out-of-plane deflection for the 3.1 MPa, no pre-load series. 24
Figure 16: Center point, out-of-plane deflection for the 3.1 MPa, 80% yield series. .. 25
Figure 17: Center point, out-of-plane velocity for the 3.1 MPa, 80% pre-load series. 26
Figure 18: Out-of-plane deflection contours for the 400°C, 3.1 MPa (a) no pre-load and (b) 80% yield cases. 28
Figure 19: Strain contours (ε_{yy}) for 400°C, 3.1 MPa cases extracted from DIC at 0.9 ms. 29

CHAPTER 2

Figure 1: (a) The geometry of the specimen used and a side view of the specimen in the fixture (b) the specimen's orientation relative to the shock tube (top view).... 40
Figure 2: (a) The location of thermocouples on the specimen. (b) A typical plot of temperature vs time for the thermocouple positions in (a). 41
Figure 3: A schematic of the shock tube is shown in the top image supplemented by images of the actual shock tube (bottom left) and a schematic of the muzzle section (bottom right). 42
Figure 4: A typical pressure profile captured for a specimen normal and 3mm from the shock tube muzzle. 42
Figure 5: The locations of the cameras in relation to the specimen along with an example of a real speckle pattern used for DIC is shown here. 44

Figure 6: Out-of-plane deflection along the center of the specimen at different time steps. 44

Figure 7: Out-of-plane deflection contours corresponding to the times shown in Figure 6. (The scales of the contours are shown at the bottom of each image.) 45

Figure 8: The out-of-plane deflection at the free edge of the specimen as a function of time for three different temperatures. 46

Figure 9: The post-mortem images for 3 different temperatures (from right to left: 800°C, 400°, 25°) for the 3mm gap, normal shock incidence series. 47

Figure 10: The out-of-plane deflection contours at room temperature for the angles of (a) 0° and (b) 30°. 48

Figure 11: The strain (ε_{xx}) contours for the 30° angle at room temperature. 49

Figure 12: The velocity (m/s) contours for the angles of (a) 0° and (b) 30°. 50

Figure 13: The free edge, out-of-plane displacements as a function of time for each experiment conducted. 51

CHAPTER 1

DYNAMIC RESPONSE OF PRE-LOADED STRUCTURES SUBJECTED TO COMBINED EXTREME ENVIRONMENTS

by

Craig Tilton, Shyamal Kishore, Prathmesh Parrikar, Arun Shukla

Prepared for submission to The Journal of Impact Engineering

Corresponding Author: Craig Tilton

University of Rhode Island

Mechanical, Industrial, and Systems Engineering

92 Upper College Road, Kingston, RI 02881

Phone: 401-487-5410

Email Address: craig_tilton@uri.edu

Abstract

An extensive series of experiments was performed on Hastelloy X plates which were subjected to combined in-plane tensile loading, transverse shock loading, and extreme temperatures. To achieve these loading conditions a shock tube apparatus was used in conjunction with a novel hydraulic pre-loading fixture and propane flame torches. In order to understand the effects of peak shock loads on the deformation phenomenon of the plates, two series of experiments were carried out at peak shock loads of 1.7 MPa and 3.1 MPa, respectively. Both series of experiments were conducted at different temperatures ranging from room temperature to 900°C. High speed photography and Digital Image Correlation (DIC) were used to obtain three-dimensional, full-field deformation. Side view images were also captured to confirm the phenomena observed. It is evident that the addition of a tensile pre-load reduces the maximum deflection for all temperatures. However, further increasing the magnitude of the aforementioned tensile load has diminishing returns for higher temperatures. It was seen that the specimen experiences a decrease in resistance to deformation caused by a blast loading for temperatures until 800°C. However, at 900°C, the specimen's resistance was observed to be greater than at 800°C. It was also observed that an indentation mode of deformation occurs at high temperatures in the case of 3.1 MPa peak load case but for no temperature in the 1.7 MPa peak load case.

Introduction

In hypersonic flight applications, structures both within gas engines as well as outer body panels can experience extreme environments. For example, critical structures within aerospace engines can experience centripetal forces up to 900 kN and temperatures in excess of 800°C [1]. It has also been observed that the surface of hypersonic vehicles traveling at Mach 5 can experience temperatures above 1000°C. [2]. Therefore, it becomes imperative that structures and materials used for aerospace applications are capable of withstanding such intense environments. One such material is Hastelloy X, a nickel-based superalloy renowned for its oxidation resistance and strength at high temperature [3]. Hastelloy X and other closely related superalloys have been used in aerospace components ranging from burner cans, turbine blades, or other exhaust-end components in aerospace engines to aerodynamically heated skin in space vehicles [4]. Therefore, due to the use of Hastelloy X in critical components of aerospace applications, it is necessary that its structural behavior is well understood in extreme environments. Certain critical components involving Hastelloy X also have pre-loads on the structure based on the application. Ample amount of research has been done on subjecting clamped beams or plates to shock loading [5-11]. Also, work of particular interest has been done on pre-loaded beams subjected to dynamic loading. Specifically, Cost and Jones analytically studied pre-loaded flat plates subjected to blast loading [12]. Also, Chen and Yu studied the influence of axial pre-load on beams subjected to transverse dynamic loads and found a transition in failure mode when pre-tension reaches a critical value [13].

A large amount of work has been done studying Hastelloy X at high temperature and quasi-static loads [14-19]. Kondo et al. [20] performed impact experiments on Hastelloy X after being subjected to high temperature helium environments for extended periods of time. Abotula et al. [21] developed a constitutive model for Hastelloy X at high temperatures under varying strain rates and found that the material experiences a decrease in yield strength up to 700°C, and then peak at 900°C before continuing to decrease. However, these studies did not utilize an air blast loading and the specimen geometry was not similar to that of critical aerospace structures. Although, Abotula et al. [22] performed high temperature, shock loading experiments on Hastelloy X plates, the study only explored the material under a simply supported boundary condition. Also, Chennamsetty et al. [23] performed shock experiments on clamped-clamped Hastelloy X at varying incident shock angles but the study did not include a tensile pre-load on the specimen. Therefore, this study seeks to explore the underlying physics related to the shock loading of Hastelloy X plates at high temperature and under tensile pre-load.

Experimental Procedures

An experimental study was designed to investigate the effect of temperature, magnitude of blast loading and pretension on the performance of Hastelloy X. Experiments were carried out at peak applied pressures of 1.7 MPa and 3.1 MPa. At least three experiments were performed for each case to ensure repeatability. For the case of 1.7 MPa loading, the experiments were carried out at 25°C, 225°C, 400°C, 600°C, 800°C, and 900°C and consisted of three pre-tension conditions, i.e., no pre-load, 50% yield strength, and 80% yield strength each, where the yield strength varies depending on the temperature of the experiment. For the case of 3.1 MPa loading, the experiments were carried out at 25°C, 400°C, 800°C, and 900°C and consisted of two loads, i.e., no pre-load, and 80% yield strength each.

Material and Specimen Geometry

The specimen material used was Hastelloy X, supplied by Haynes International. Hastelloy X is primarily composed of Ni, Cr, Fe, and Mo and is known for its strength at high temperatures and oxidation resistance. In the present study, rectangular plates measuring 2 in (50.8 mm) wide, 8 in (203.2 mm) long and 0.0625 in (1.5875 mm) thick were used. Two 0.5 in (12.7 mm) holes were drilled in the specimens 0.5 in (12.7 mm) from each edge in order to clamp the specimen in its position in the fixture. The unsupported length of the specimen was 6in (152.4mm).

Pre-Load Apparatus

A novel apparatus (Figure 1) was developed such that the specimen could be subjected to high temperature, tensile pre-load, and shock loading. In order for the fixture to apply the in-plane, tensile pre-load, a hydraulic cylinder was used in series with the specimen. During heating, the hydraulic cylinder was placed in a neutral position to allow the specimen to thermally expand freely. The hydraulic cylinder was used in the cases where no pre-load was applied to allow for free thermal expansion as to not pre-stress the specimen. Once the hydraulic cylinder reached its final position post thermal expansion and application of the pre-load, the hydraulic cylinder was locked firmly to minimize movement. Rollers were used between the cylinder and the specimen to prevent transverse deformation of the loading apparatus. A strain transducer affixed to the loading setup was used to measure the applied in-plane load. Due to high temperatures experienced by the fixture during the heating of the specimen, a cooling system was used around the transducer to ensure hot, ambient air did not affect it. Bolt fasteners through the holes in the specimen and clamps were used to secure the specimen at both ends rigidly, and serrations machined into the clamps transferred the tensile pre-load to the specimen and prevented slipping during the shock loading.

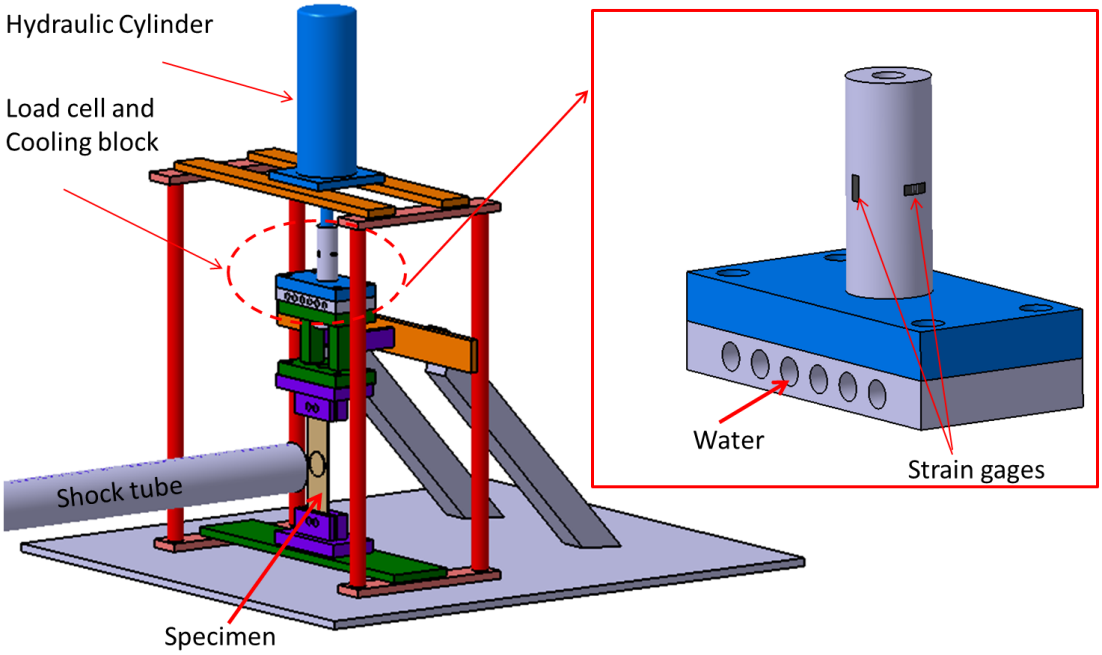

Figure 1: Novel tensile pre-load apparatus developed for these experiments.

High Temperature

To simulate the high temperatures in an extreme environment, propane heating torches were chosen to heat the Hastelloy X specimens. The use of propane heating torches has been established by Abotula et al [22] and proven to be a robust, non-contact method of achieving uniform temperatures across the specimen. Prior to conducting an experiment, a calibration step was carried out wherein the required temperature was achieved via adjusting the propane pressure and flow output through the nozzles along with adjustments to the nozzle orientations. To monitor temperature uniformity across the specimen, nine thermocouples were attached to a calibrating specimen on the opposite side from where the flames were applied. The calibration was carried out until a temperature gradient across each of the nine thermocouples was less than ±10% of the desired steady-state temperature. The location of the thermocouples is shown in Figure 2a and a typical graph of the temperature

distribution is shown in Figure 2b. In Figure 2b, steady state is reached after approximately 2 minutes of heating, which was typical of all the experiments conducted. After calibrating the heating setup and noting the time taken to reach steady state, multiple experiments could be conducted without requiring re-calibration.

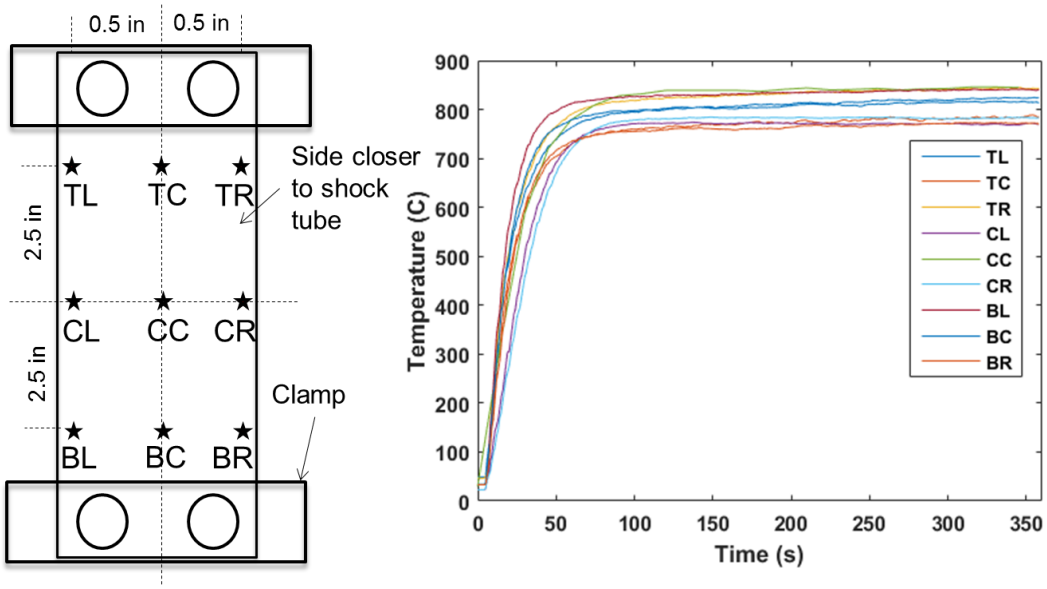

Figure 2: (a) Thermocouple locations (b) Typical temperature distribution.

Shock Tube

A shock tube apparatus (Figure 3a) was used to subject the center of the specimen to the desired shock loading. The shock tube has a driver and a driven section separated by a disposable diaphragm. The driver section is pressurized using Helium gas until a critical pressure gradient across the sections is reached and the diaphragm bursts allowing the pressurized gas to rapidly flow down the length of the shock tube. The rapid release of gas traveling down the converging phase of the driven section creates a shock wave which then travels further to be incident on the specimen. In the present study, the diaphragm was made up of one or two, 10 mil (0.254mm) Mylar sheets depending on the peak shock pressure required. A typical pressure

profile of the shock loading is shown in Figure 4. The typical incident and reflected pressure values were 0.5 MPa and 1.6 MPa respectively for the 1 ply experiments and 1.7 MPa and 3.1 MPa respectively for the 2 ply experiments.

The shock tube muzzle section (Figure 3b) has a diameter of 38.1mm and is located 3mm from the specimen. The muzzle is mounted with PCB102A pressure sensors to record the pressure event. The pressure sensors are located 20mm, 60mm, and 180mm from the end of the muzzle.

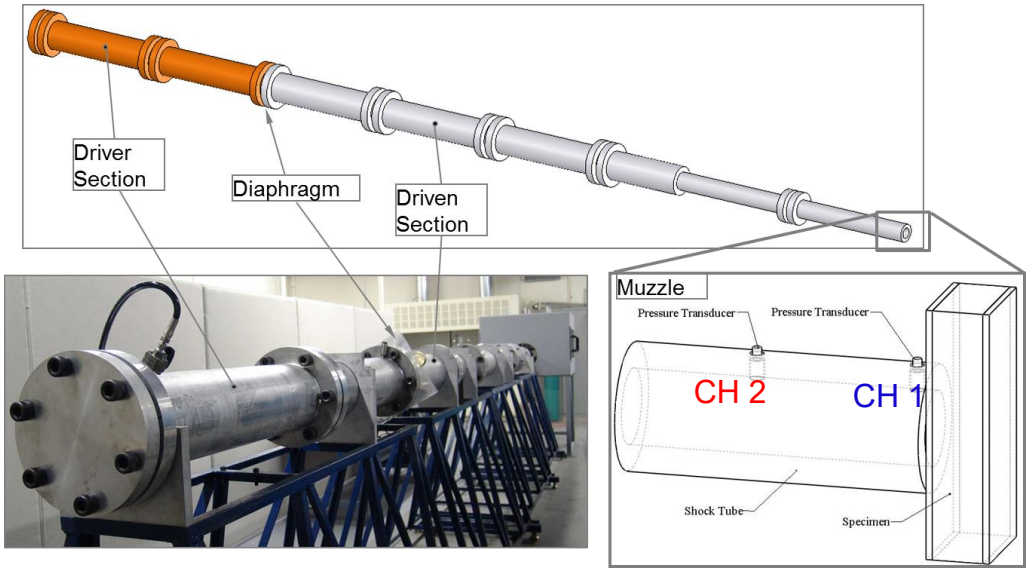

Figure 3: Shock tube apparatus and muzzle (a) actual (b) schematic.

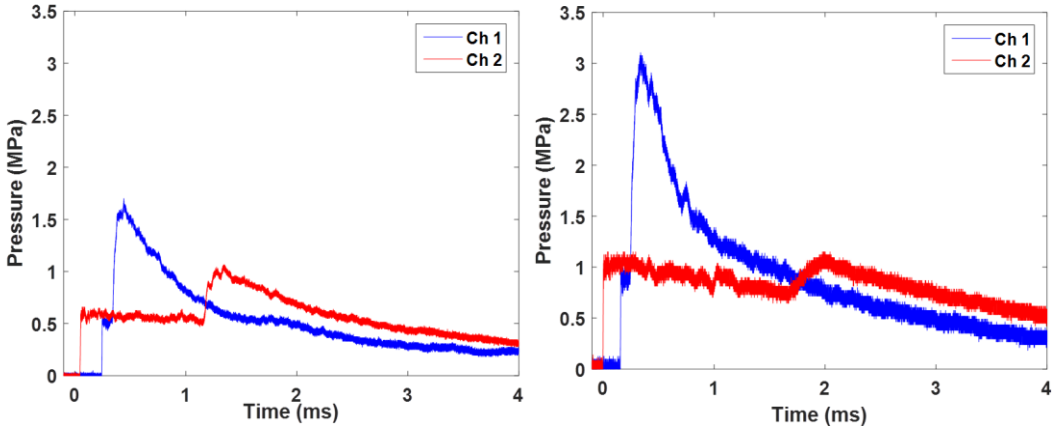

Figure 4: (a) 1.7 MPa pressure profile (b) 3.1 MPa pressure profile.

High Speed Photography System

A high speed photography system consisting of three cameras (figure 5) was used to capture the event at 50,000 fps. Two cameras at the rear of the specimen outfitted with blue bandpass filters were used in conjunction with a high intensity light source in order to capture images used for Digital Image Correlation (DIC). This method was first implemented by Abotula et. al. [22] and was proven to be a robust, effective method of capturing images. The specimens were speckled using high temperature resistant paint for the DIC method. The third camera was placed on the side of the specimen to validate the DIC and capture any other necessary information. The high-speed photography system and light source were triggered using the incident pulse registered by the oscilloscope. Although the cameras were calibrated for DIC based on the refractive index of room temperature air, the DIC method is robust and valid at high temperatures due to the fact that a high temperature reference pre deformation image was used, minimizing the error due to the change in refractive index when comparing air to propane. Also, a side view camera is utilized in order to validate the corresponding deformation evaluated by the DIC method.

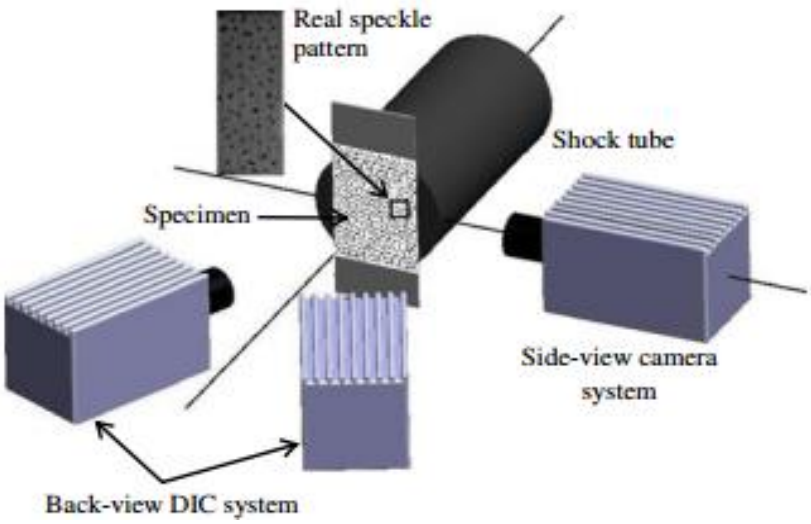

Figure 5: Camera locations for digital image correlation and side view.

Results and Discussion

The 1.7 MPa experiments were conducted at temperatures of 25°C, 225°C, 400°C, 600°C, 800°C, and 900°C. However, 3.1 MPa experiments were conducted only at 25°C, 400°C, 800°C, and 900°C and the experiments for the temperatures 225°C and 600°C were excluded. These temperatures, were found to be the transition temperatures at which no significant differences in structural response were observed

A. Shock pressure: 1.7 MPa, pre-load: no pre-load.

Typical deformation images recorded are shown in Figures 6 and 7. Figure 6 shows the side view of the specimen, while Figure 7, obtained from DIC, shows the back-face, out-of-plane contours of the specimen, as the specimen deflects away from the shock tube muzzle and towards the cameras.

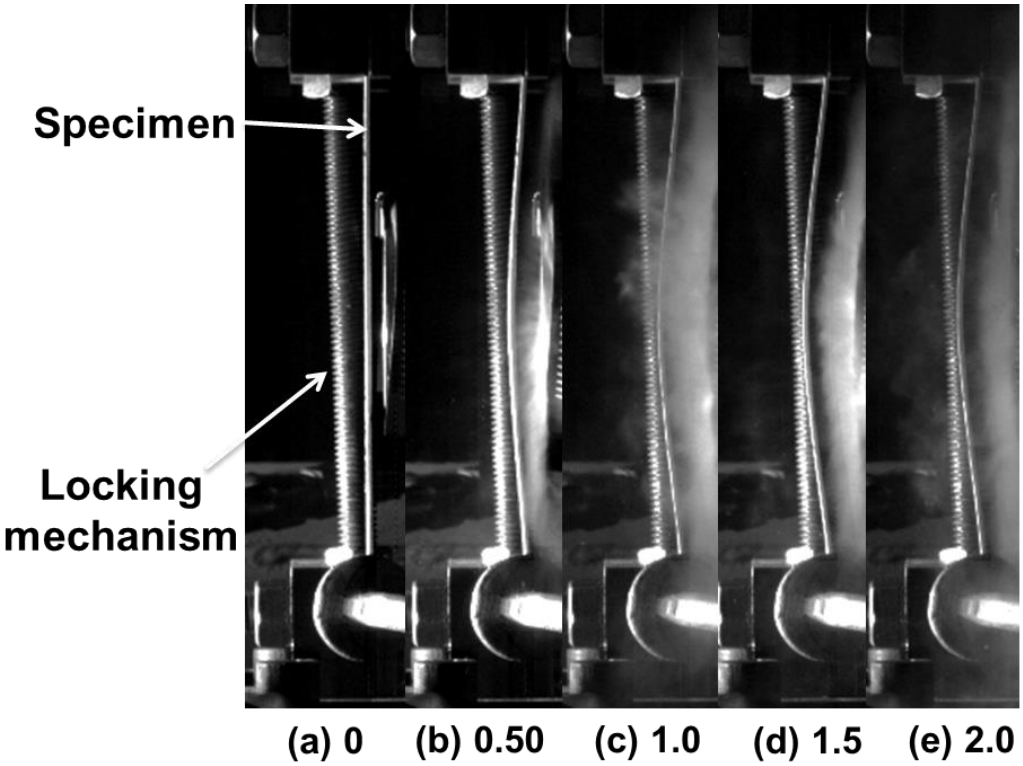

Figure 6: Side view images of a room temperature, no pre-load experiment. The numbers indicate the time in ms from when the incident pulse triggered the cameras.

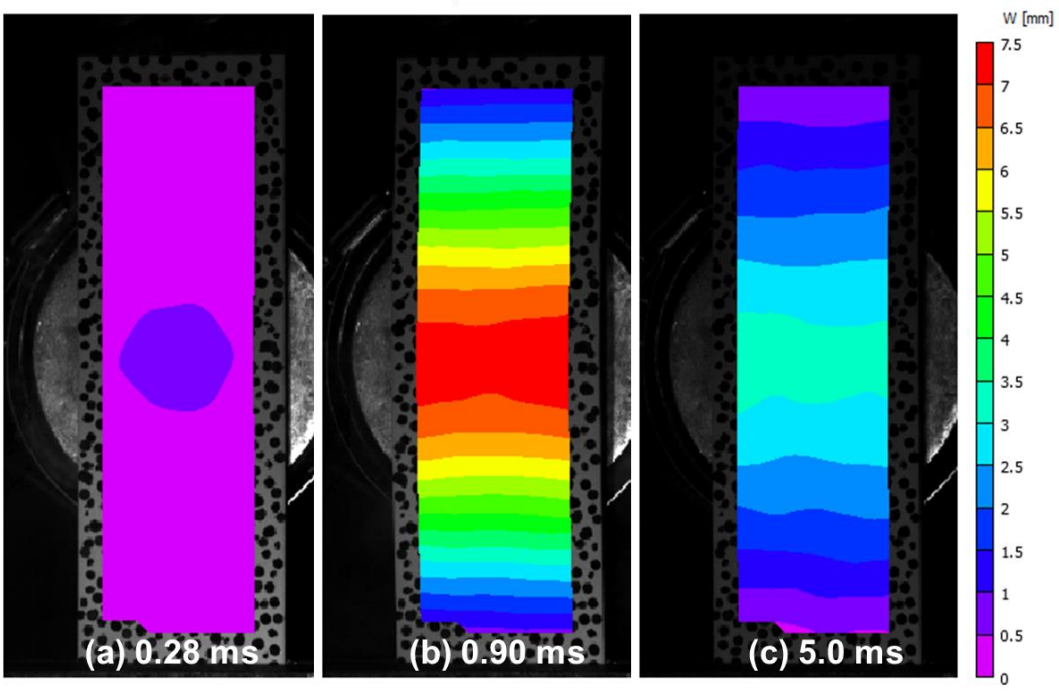

Figure 7: Out-of-plane deflection contours from DIC for a room temperature, no pre-load experiment.

In figure 7, once the shock impinges on the specimen, the specimen undergoes a transient indentation in the center during a local deformation phase (a). This local indenting is the same size as the loading area and only lasts for 0.40 ms before being eclipsed by the rapidly evolving global deformation across the center. This local indentation followed by the global deformation phase (b), is driven by the inertial effects caused by the loading. At this point, the deformation across the width of the specimen is uniform and, therefore, the transient indentation is clearly absent. Finally, the specimen reaches its maximum deformation and begins to oscillate about its bowed position (c). These three phases of deformation were also observed for all other temperatures of the 1.7 MPa, no pre-load case.

From the DIC, as shown in Figure 7, out-of-plane deflection can be extracted. The following figure (Figure 8) shows the center point, out-of-plane deflection as a function of time for each temperature at which experiments were conducted.

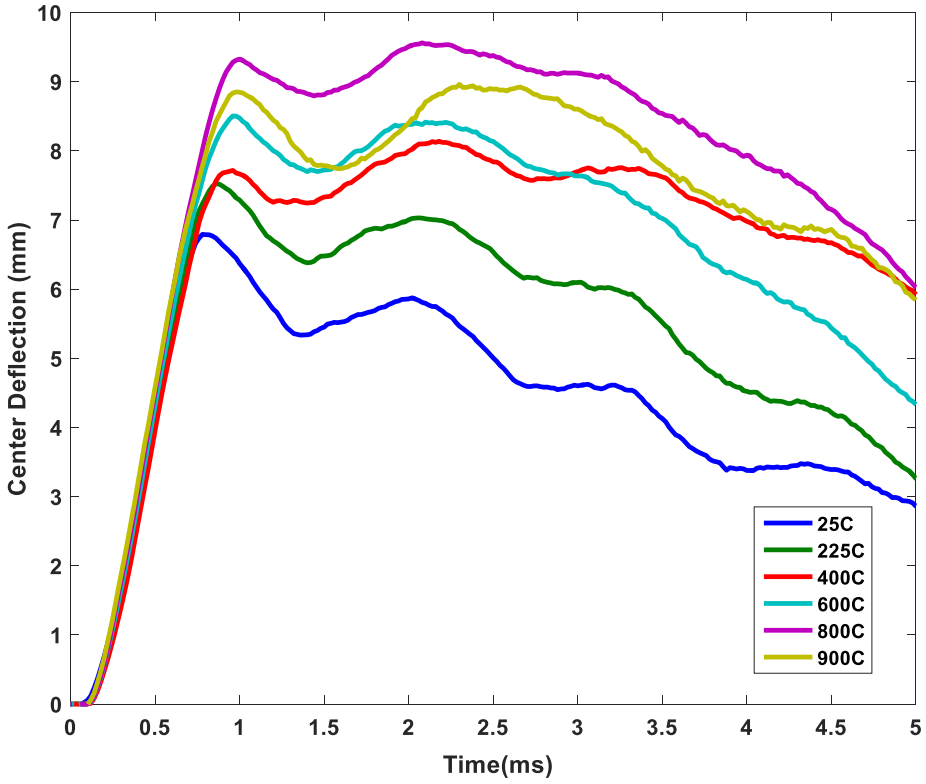

Figure 8: Center point, out-of-plane deflection for the 1.7 MPa, no pre-load series.

It should be noted that for the experiments at 25 °C and 225°C, the maximum deflection occurs during the first oscillation and, therefore, the first peak is greater than the second peak. However, in the experiments conducted at 400°C and higher, the second peak is very similar to, if not greater, than the first peak. Once the specimen reaches its maximum deflection, there is a large amount of force pulling down on the hydraulic cylinder. Due to the fact that there is no hydraulic pressure for this series, the downward force causes the top clamp of the fixture to move down about 1 mm and this can be seen from the DIC data. Therefore, as the specimen

begins to oscillate, the specimen is able to deform further than the previous maximum. Thus, the movement of the top clamp causes the second peak to be equal or higher than the first peak.

It is observed that the maximum out-of-plane deflection increases as temperature is increased up to 800°C. This behavior can be easily explained from the decrease in yield strength of Hastelloy X with increasing temperature up to 750°C as seen in Figure 9. The yield strength as a function of temperature is shown in Figure 9a where the blue, solid curve is the quasi-static yield strength [24] and the red, dashed curve is the high strain rate yield strength [22].

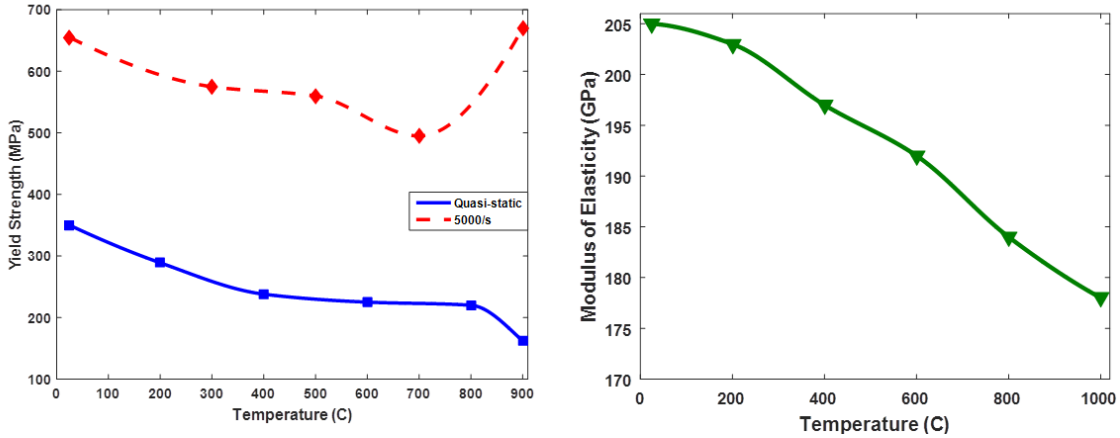

Figure 9: (a) Yield strength as a function of temperature for Hastelloy X where the solid, blue curve is a quasi-static strain rate [24] while the dashed, red curve is a high strain rate (5000/s) [22]. (b) Dynamic modulus of elasticity as a function of temperature for Hastelloy X [3].

However, the maximum deflection at 900°C is less than that of 800°C. This anomaly has been observed in many previous works studying the constitutive behavior of Hastelloy X, but this anomaly in the structural response of Hastelloy X plates has not been reported before. This anomaly can be directly related to the high strain rate yield plot shown in Figure 9. Abotula et al. [21] explain that an increase in yield

strength at higher temperatures is caused by three important factors namely (i) Grain boundary embrittlement, (ii) deformation mechanisms, and (iii) γ′ coarsening. Abotula et al. also explains the contribution of the ratio of intergranular to transgranular cracks and how this changes with temperature causing changes in the yield strength of the material.

B. Incident pressure: 1.7 MPa, pre-load: 50% yield.

The observed phases of deformation, in this case, are the same as in the case of 1.7 MPa, no pre-load case, as illustrated in Figure 8. When looking at the out-of-plane center point deflection (Figure 10), it can be seen that the second peak is not greater than the first peak for all temperatures. Recall that in the previous section, it was discussed that the second peak was due to the hydraulic pressure not being able to prevent clamp movement in the context of the no pre-load condition. In the 50% yield pre-load case, however, the load applied has adequate resistance to the downward movement such that the second peak is always lower than the first peak.

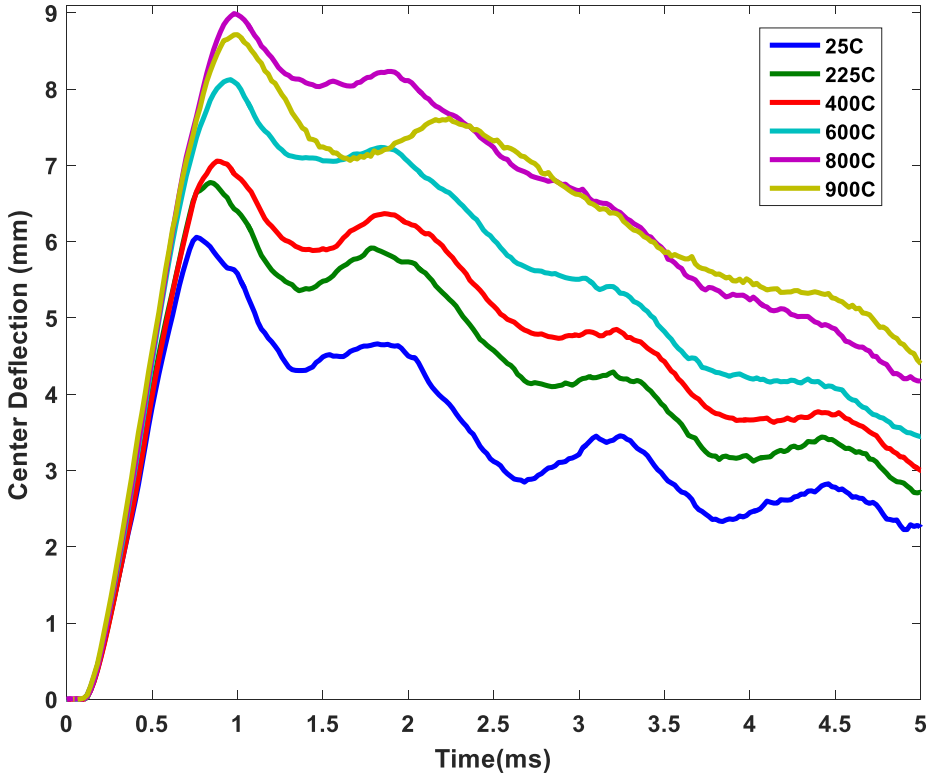

Figure 10: Center point, out-of-plane deflection for the 1.7 MPa, 50% yield pre-load series.

As seen in the no pre-load condition, the 50% yield pre-load experiments also show that the maximum deflection of the 900°C case is lower than that of the maximum deflection seen in the case of 800°C. This indicates that at higher temperatures the higher yield strength of the material plays a role in the structural response of the material despite the addition of a tensile pre-load of 50% of the yield strength.

C. Incident pressure: 1.7 MPa, pre-load: 80% yield.

For the case of 1.7 MPa pressure and 80% pre-load, the phases of deformation are the same as those described in section A (Figure 8). Similar to the both previous

scenarios, and shown in Figure 11, the 80% yield pre-load experiments also show that the maximum deflection of the 900°C case is lower than that of the maximum deflection seen in the case of 800°C. As previously stated this result indicates that at higher temperatures the higher yield strength of the material plays a role in the structural response of the material despite the increased magnitude of the tensile pre-load to 80% of the yield strength.

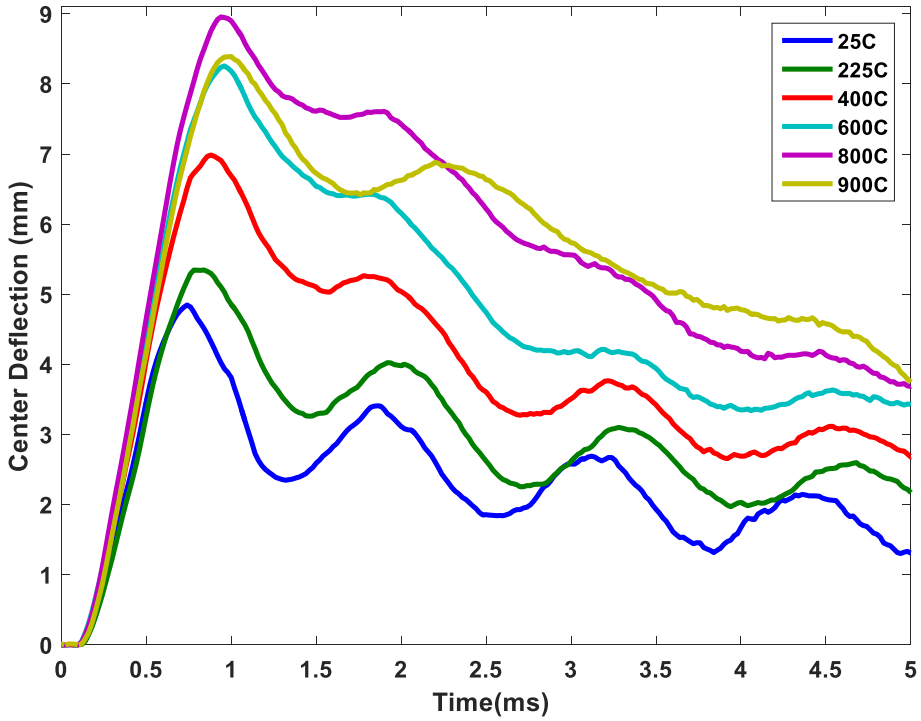

Figure 11: Center point, out-of-plane deflection for the 1.7 MPa, 80% yield series.

D. Incident pressure: 1.7 MPa, all loads

In order to compare the deformation for all three 1.7 MPa cases, Figure 12 shows the maximum, center point, out-of-plane deflection for each temperature.

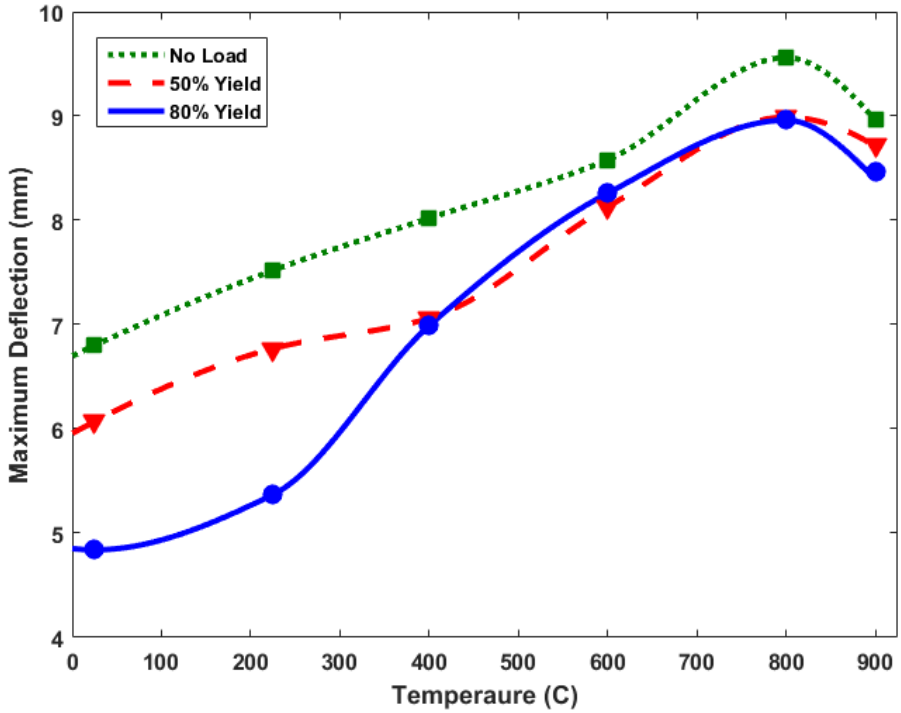

Figure 12: The maximum, center point, out-of-plane deflection as a function of temperature for the three pre-load scenarios.

It is evident that the addition of a tensile pre-load (of magnitude equal to or greater than 50% of the yield strength value at a given temperature) reduces the out-of-plane deflection for all temperatures up to 900°C. However, increasing the magnitude of the aforementioned tensile pre-load has diminishing returns for temperatures higher than 400°C. The structural response beyond 400°C, is not significantly enhanced by increasing the tensile pre-load from 50% to 80% because the depreciated yield strength at temperatures greater than 400°C is falls below the stresses induced due to the shock load, which results in the shock loading easily and quickly pushing the stresses in the specimen beyond the yield point into the plastic flow region. The structural implication is that the resistance offered to the shock loading of the specimen is similar beyond 400°C for the cases of 50% and 80% tensile

pre-load. This phenomenon can be confirmed by the work done by Abotula et. al [22] where is was found that the flow stress of Hastelloy X decreases with temperature.

E. Incident pressure: 3.1 MPa, pre-load: no pre-load.

In Figure 8, the phases of deformation were established for a typical 1.7 MPa experiment. For the case of 3.1 MPa pressure, no pre-load, similar phases of deformation are observed but only for the experimental temperatures, 25°C and 400°C. However, for 800°C and 900°C, the typical phases of deformation are shown in Figure 13, which shows the out-of-plane contours from DIC. The contours shown in Figure 13 shows the 800°C experiments, but the phases of deformation and contour plots for 900°C are also similar.

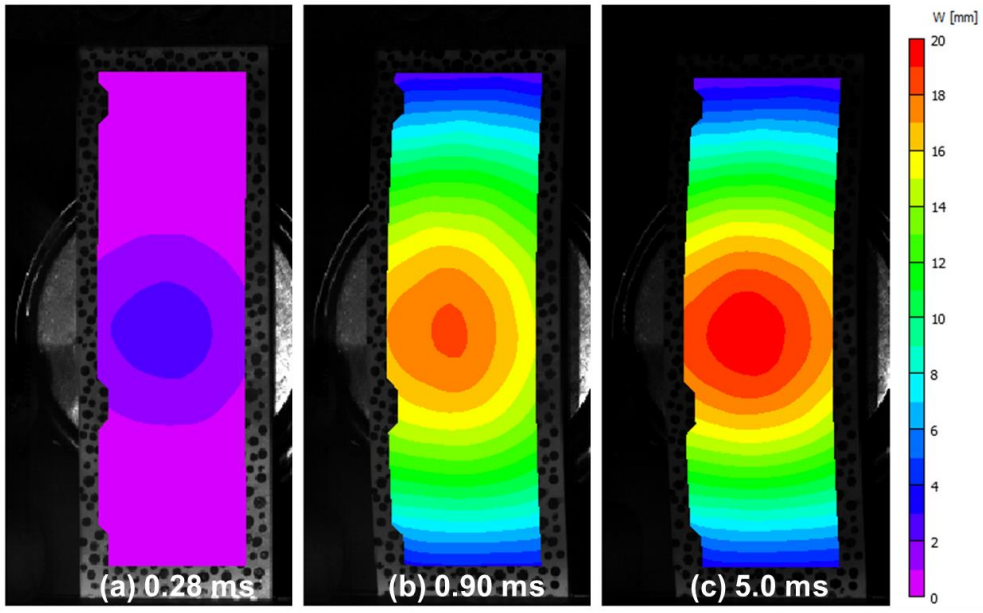

Figure 13: Out-of-plane deflection contours from DIC for an 800°C, no pre-load experiment.

Similar to the case of 1.7 MPa peak load experiments, the deformation also begins with a local indentation caused by the shock loading (a). However, due to the

relatively higher load, the overall magnitude of deformation in the local indention is larger. In (b), it can be observed that the deflection across the width of the specimen in the center is not uniform even after 0.9 ms. In the 1.7 MPa case, the same time interval showed a constant deflection across the width of the specimen. Even after the specimen reached its maximum deflection point and began oscillations (c), the indention is still present. This may be defined as an indention mode of deformation; i.e., development of a local zone of protuberance across the width of the specimen even after the global deformation phase is fully developed. The indentation mode of deformation can be explained as being an artifact of the ratio between the yield stress of the material and the applied load. Due to the fact that the load applied at the center is large enough such that the transient indentation can continue into the plastic range when the stresses in the center of the specimen exceed the critical yield stress value at a given temperature. It is known that the yield stress decreases until 750°C and, therefore, the decrease in yield stress allows indentation to take place for higher temperature experiments.

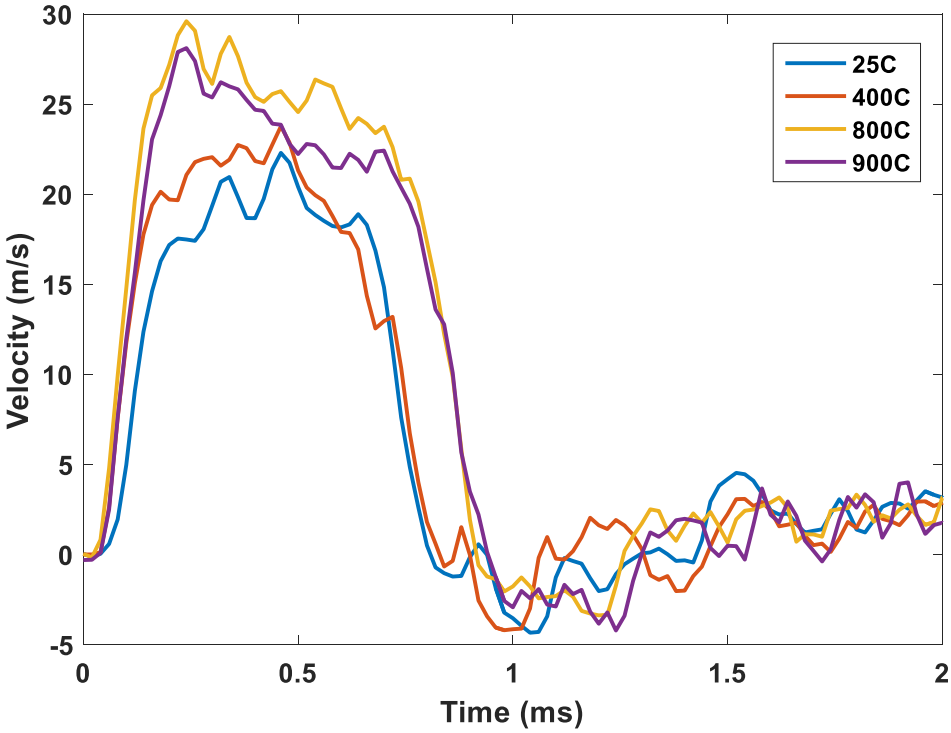

Figure 14: Center point, out-of-plane velocity for the 3.1 MPa, no pre-load series.

As previously established, for this series, indentation occurs at 800°C and 900°C. In Figure 14, it is observed that when indentation occurs, the maximum velocity of the center-point occurs earlier in time than compared to temperatures where indentation does not occur. When indentation occurs, the maximum velocity is reached at around 0.24 ms. However, for cases where indentation does not occur, the velocity reaches a maximum at around 0.44 ms. This is because the indentation mode of deformation causes the structure to quickly reach the plastic regime locally and therefore, the fall in structural rigidity allows the structure to deform with a higher acceleration before the rest of the structure's inertia slows the velocity.

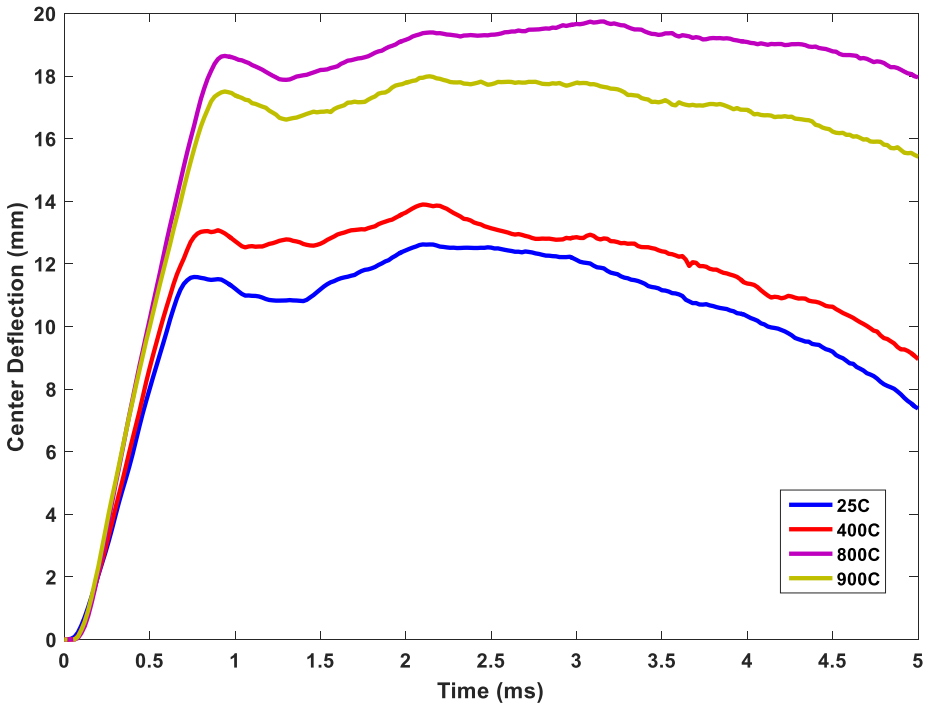

Figure 15: Center point, out-of-plane deflection for the 3.1 MPa, no pre-load series.

As previously discussed, the maximum, out-of-plane deflection of the 800°C cases is higher than that of the 900°C due to the yield stress anomaly discussed by [22].

F. Incident pressure: 3.1 MPa, pre-load: 80% yield.

When the tensile pre-load is increased from zero to 80% of the yield for the 3.1 MPa case, the center point, out-of-plane deflection can be plotted and is shown in Figure 16.

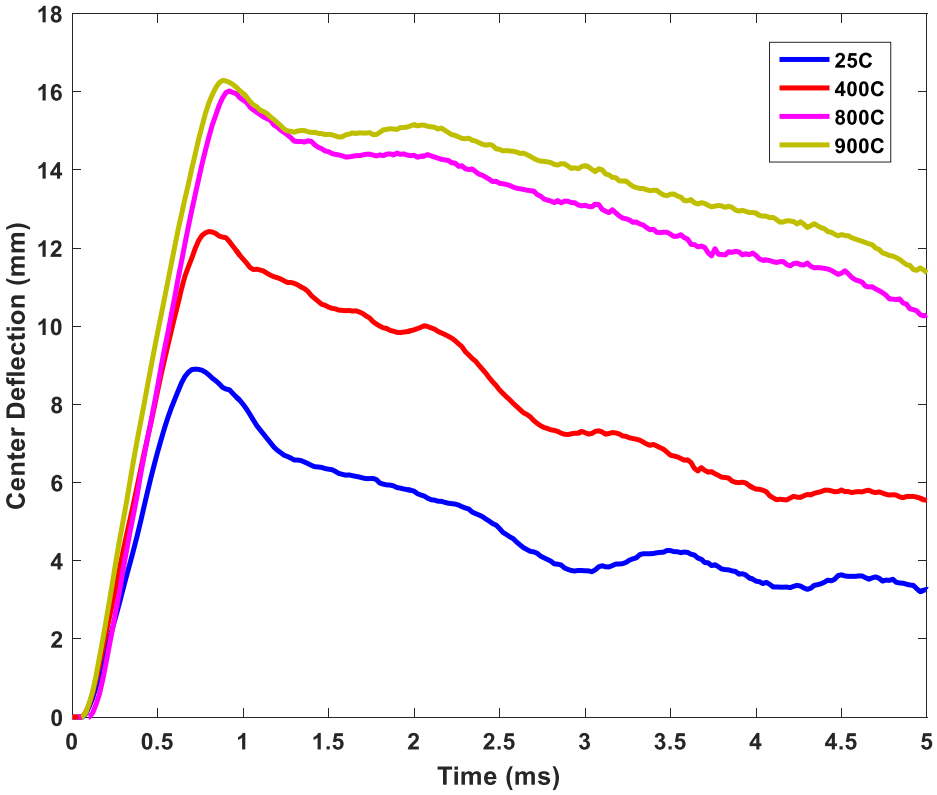

Figure 16: Center point, out-of-plane deflection for the 3.1 MPa, 80% yield series.

In all of the aforementioned experiments, the maximum out-of-plane deflection of 800°C was greater than that of 900°C. However, in Figure 16, it is apparent that the maximum deflection of 800°C and 900°C are approximately equal. When the pre-load is applied, there is an initial strain in the material before contact with the shock. This pre-strain, combined with the increased magnitude of the shock in the 3.1 MPa series causes the deformation mechanism which typically would cause a yield stress anomaly to be suppressed. The strain in the specimen is past the yield strength to a point where strain hardening is the dominant mechanism as opposed to low strains where the time in which the specimen begins to plastically deform would dominate the deformation.

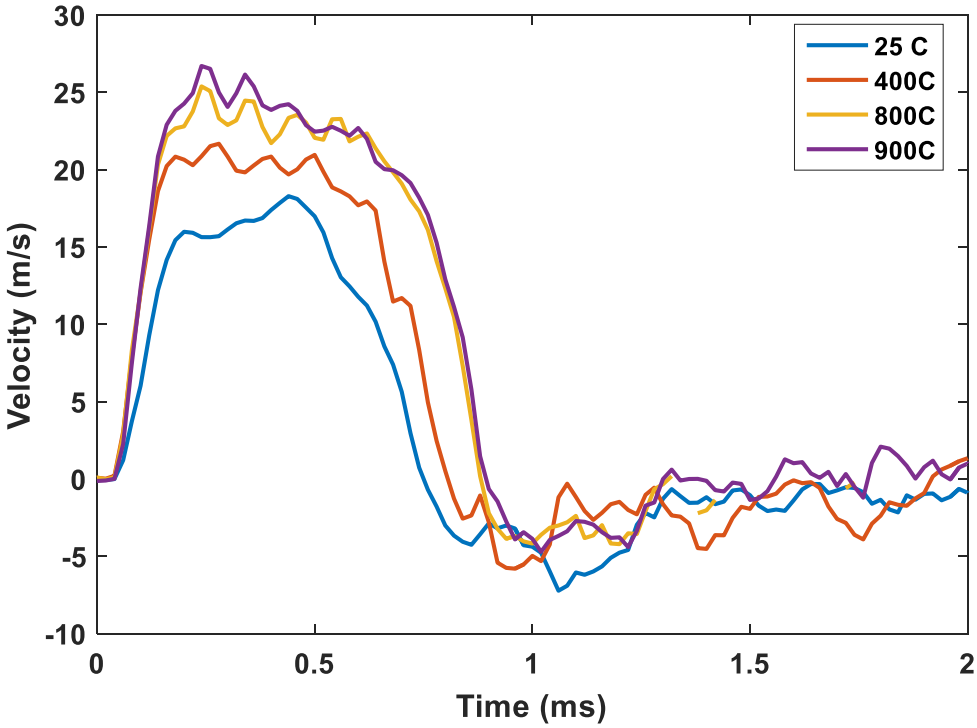

Figure 17: Center point, out-of-plane velocity for the 3.1 MPa, 80% pre-load series.

It was previously stated that for experiments where indentation occurs, the maximum velocity occurs earlier in time as compared to experiments where indentation does not occur. In Figure 17, it can be seen that the peak velocity for experiments at 25°C occurs later in time than 400°C, 800°C, and 900°C which would imply that indentation occurs at 400°C, 800°C, and 900°C. In the previous 3.1 MPa experiment series where no pre-load was applied, indentation occurred for only the 800°C and 900°C but not at 25°C and 400°C. However, when a pre-load of 80% yield is applied indentation occurs at 400°C, 800°C, and 900°C. The following section will compare the 3.1 MPa experiments in greater detail.

G. Incident pressure: 3.1 MPa, all loads.

For all the 1.7 MPa experiments, no indentation was observed. However, for 3.1 MPa experiments, the indentation mode of deformation is seen some of the time. The following table (Table 1) summarizes when indentation occurs for 3.1 MPa experiments with a "Y" indicating indentation and "N" indicating otherwise.

Table 1: This table displays whether or not indentation occurred with a "Y" indicating that indentation did occur.

3.1 MPa Pressure	No pre-load	80% pre-load
25°C	**N**	**N**
400°C	**N**	**Y**
800°C	**Y**	**Y**
900°C	**Y**	**Y**

It can be seen that for the 400°C cases, indentation occurs only when a pre-load was applied. It is apparent from the DIC images in Figure 18 that the out-of-plane deflection observed is constant across the width for the no pre-load case, but not constant for the 80% yield case. It can be seen that at 0.38 ms, the no pre-load case begins to be dominated by the global deformation over the local incipient indentation mode. However, at the same time step, the 80% yield pre-load case continues to be locally deformed. Later in time, at 0.9 ms, it is evident that the no pre-load case has made the full transition to global deformation, but the deflection in the 80% case is not constant across the width. Due to the fact that indentation has occurred at the same temperature (400°C) and similar deflections were observed, the strain profiles of the 400°C can be readily compared. The strain profiles (ε_{yy}) extracted from DIC are shown in Figure 19. From Figure 19, it is apparent that the onset of indentation causes a larger area of maximum strain (ε_{yy}) as compared to the area of maximum strain caused by global deformation. This larger area of maximum strain is caused by the

localized stretching of the plate due to indentation. Also, note that the strain in the global deformation image is not constant across the width of the specimen. This is due to some small local maximums and minimums due to the plate not deflecting perfectly outward but rather locally vibrating throughout the deformation. In the case of strain, the small deformations are noticeable due to the small scale on which strain is shown.

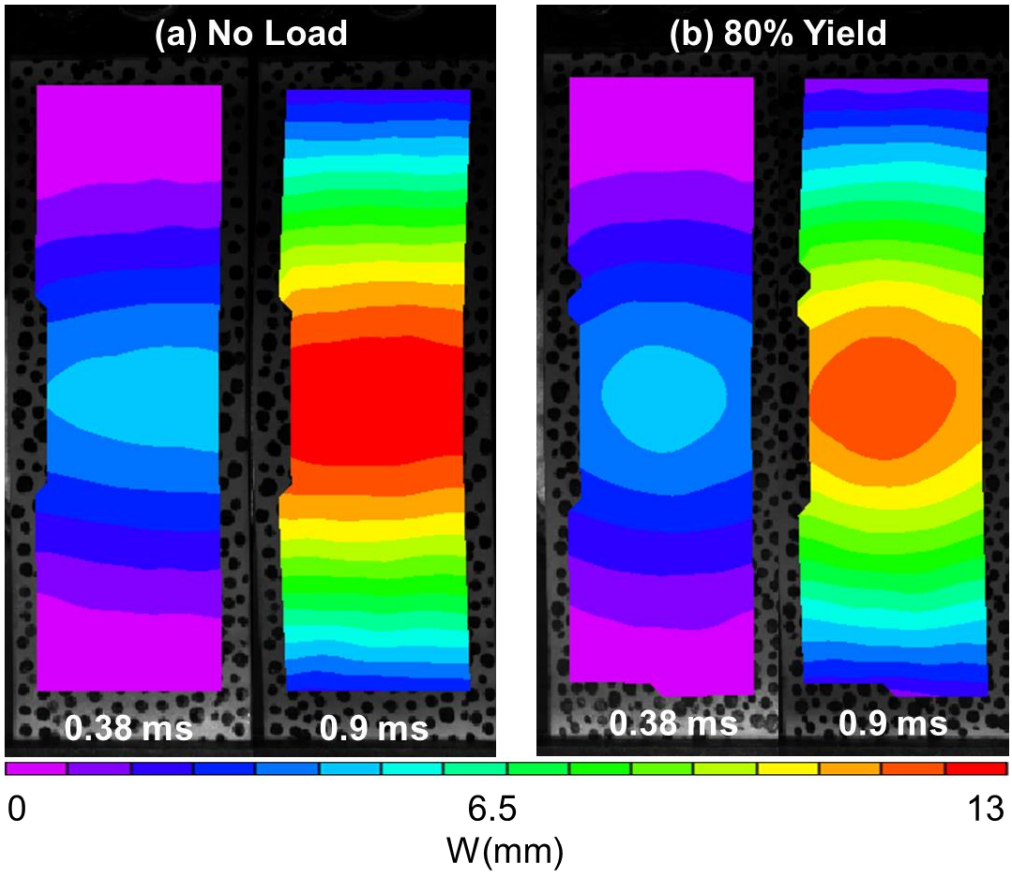

Figure 18: Out-of-plane deflection contours for the 400°C, 3.1 MPa (a) no pre-load and (b) 80% yield cases.

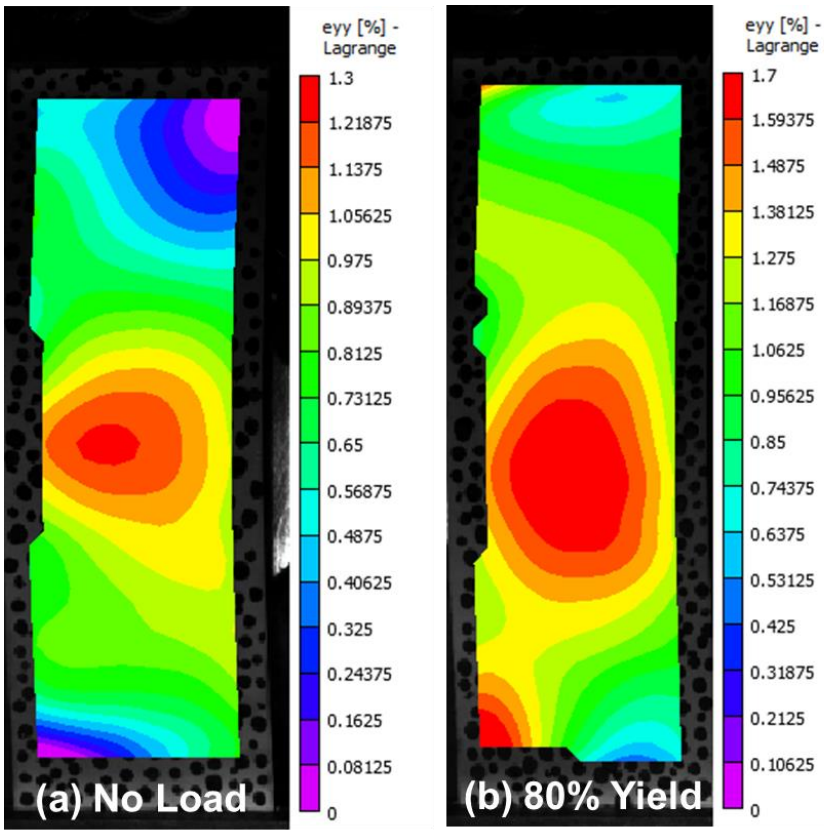

Figure 19: Strain contours (ε_{yy}) for 400°C, 3.1 MPa cases extracted from DIC at 0.9 ms.

Conclusions

A comprehensive series of experiments were conducted subjecting Hastelloy X plates to a combination of extreme environments. Experiments were conducted at temperatures up to 900°C, tensile pre-loads up to 80% of the yield stress of the material, and shock loads up to 3.1 MPa. Digital Image Correlation and high speed photography were used to develop an understanding of the structural behavior of the material when subjected to such extreme environments. Through these experiments, the following major conclusions have been drawn:

- A novel fixture was developed robust enough to withstand high temperature and shock loading while applying a tensile pre-load.
- The yield strength anomaly found to be a material property is verified at a structural level.
- The yield strength anomaly occurs in the structure for all tensile loads at low incident shock pressures.
- The yield strength anomaly is not the dominate mode of structural deformation when both high incident shock pressures and tensile loads are applied.
- The application of a tensile load reduces the deflection of the plates to shock, but increasing the magnitude of the tensile load has no effect on the out-of-plane deflection.
- The onset of indentation is a function of the temperature, shock pressure, and tensile pre-load applied.

Acknowledgements

The authors would like to thank Air Force Office of Scientific Research (AFOSR) under Grant No. FA9550-13-1-0037. The authors would also like to thank their colleagues in the Dynamics Photo-Mechanics Laboratory.

References

[1] Spittle, P., (2003). Gas turbine technology, *Physics Education*, 38(6):504-511.

[2] Rabinowicz, J., (1957). Aerodynamic studies in the shock tube, Ph.D. Thesis, California Institute of Technology, USA.

[3] Haynes, International, Jan 2016. http://www.haynesintl.com/pdf/h3009.pdf

[4] Donachie, M., Donachie, S., (2002). Superalloys a technical guide. Materials Park, OH: ASM International.

[5] Menkes, S., Opat, H., (1973). Broken beams. *Experimental Mechanics* 13, 480-486.

[6] Nurick, G. N., & Shave, G. C. (1996). The deformation and tearing of thin square plates subjected to impulsive loads - An experimental study. *International Journal of Impact Engineering*, *18*(1), 99–116.

[7] Balden, V. H., & Nurick, G. N. (2006). Numerical simulation of the post-failure motion of steel plates subjected to blast loading. *International Journal of Impact Engineering*, *32*(1-4), 14–34.

[8] Jacob, N., Nurick, G. N., & Langdon, G. S. (2007). The effect of stand-off distance on the failure of fully clamped circular mild steel plates subjected to blast loads. *Engineering Structures*, *29*(10), 2723–2736.

[9] Wierzbicki, T., Nurick, G.N., (1996). Large deformation of thin plates under localised impulsive loading. *International Journal of Impact Engineering* 18, 899-918.

[10] Yuan, Y., & Tan, P. J. (2013). Deformation and failure of rectangular plates subjected to impulsive loadings. *International Journal of Impact Engineering*, *59*, 46–59.

[11] Veldman, R. L., Ari-Gur, J., & Clum, C. (2008). Response of pre-pressurized reinforced plates under blast loading. *International Journal of Impact Engineering*, *35*(4), 240–250.

[12] Cost TL, Jones HW (1979) Dynamic response of blast loaded prestressed flat plates. *Journal of Sound and Vibration* 62(1):111–120

[13] Chen FL, Yu TX (2000) Influence of axial pre-load on plastic failure of beams subjected to transverse dynamic load. *Advanced Engineering Plasticity* 177(1):255–260

[14] Swaminathan, B., Abuzaid, W., Sehitoglu, H., & Lambros, J. (2014). Investigation using digital image correlation of Portevin-Le Chatelier in Hastelloy X under thermo-mechanical loading. *International Journal of Plasticity*, *64*, 177–192.

[15] Sakthivel, T., Laha, K., Nandagopal, M., Chandravathi, K. S., Parameswaran, P., Panneer Selvi, S., Mannan, S. K. (2012). Effect of temperature and strain rate on serrated flow behaviour of Hastelloy X. *Materials Science and Engineering A*, *534*, 580–587.

[16] Aghaie-Khafri, M., & Golarzi, N. (2008). Forming behavior and workability of Hastelloy X superalloy during hot deformation. *Materials Science and Engineering: A*, *486*(1-2), 641–647.

[17] Lai, G. Y. (1978). An investigation of the thermal stability of a commercial Ni-Cr-Fe-Mo alloy (hastelloy alloy X). *Metallurgical Transactions A*, *9*(6), 827–833.

[18] Rowley M.A., Thornton E.A., (1996). Constitutive modeling of the visco-plastic response of Hastelloy-X and Aluminium alloy 8009. *Journal of Engineering Materials and Technology*, 118:19–27.

[19] Kim, W. G., Yin, S. N., Ryu, W. S., Chang, J. H., & Kim, S. J. (2008). Tension and creep design stresses of the "Hastelloy-X" alloy for high-temperature gas cooled reactors. *Materials Science and Engineering A*, *483-484*(1-2 C), 495–497.

[20] Kondo, Y., Fukaya, K., Kunitomi, K., & Miyamoto, Y. (1988). Tensile and impact properties changes of HASTELLOY X after exposure in high-temperature helium environment. *Metallurgical Transactions A*, *19*(5), 1269–1275.

[21] Abotula S., Shukla A., Chona R., (2011). Dynamic constitutive behavior of Hastelloy X under thermo-mechanical loads, *Journal of Material Science*, 46(14):4971–4979.

[22] Abotula, S., Heeder, N., Chona, R., & Shukla, A. (2013). Dynamic Thermo-mechanical Response of Hastelloy X to Shock Wave Loading. *Experimental Mechanics*, *54*(2), 279–291.

[23] Chennamsetty, A. R. K., LeBlanc, J., Abotula, S., Naik Parrikar, P., & Shukla, A. (2015). Dynamic response of Hastelloy® X plates under oblique shocks: Experimental and numerical studies. *International Journal of Impact Engineering*, *85*, 97–109.

[24] Brinkman, C., Rittenhouse, P., Corwin, W., Strizak, J., Lystrup, A., DiStefano, J.R., (1976). Application of Hastelloy X in gas-cooled reactor systems. *Oak Ridge National Laboratory Annual Report*. Metals and Ceramics Division, October 1976.

CHAPTER 2

DYNAMIC RESPONSE OF CANTILEVERED STRUCTURES SUBJECTED TO OBLIQUE SHOCK & EXTREME TEMPERATURES

by

Craig Tilton, Shyamal Kishore, Prathmesh Parrikar, Arun Shukla

Prepared for submission to Experimental Mechanics

Corresponding Author: Craig Tilton

University of Rhode Island

Mechanical, Industrial, and Systems Engineering

92 Upper College Road, Kingston, RI 02881

Phone: 401-487-5410

Email Address: craig_tilton@uri.edu

Abstract

A comprehensive series of experiments was performed subjecting cantilevered Hastelloy X plates to extreme temperatures as well as oblique, transverse shock loads. A shock tube was used to achieve consistent planar shock waves and was supplemented by four propane torches to obtain high specimen temperatures. To capture the deformation event, high speed photography was used in conjunction with Digital Image Correlation to attain full-field, three-dimensional deflections, velocities, and strains. Experiments were conducted at temperatures of 25°C, 400°C, and 800°C and shock angles of 0° (normal), 15°, and 30°. It is evident that an increase in temperature causes an increased magnitude in out-of-plane deflection and in certain cases causes the deformations to occur in mode II. It is also observed that increasing the angle of the specimen relative to the shock decreases the magnitude of out-of-plane deformation.

Introduction

In a typical hypersonic aerospace vehicle's engine, the combustor-end components can reach temperatures in excess of 800°C [1]. Therefore, these critical components are made from Ni-based superalloys, one of which being Hastelloy X. Superalloys must be used due to the fact that they retain their strength at extreme temperatures. These critical components may also experience unwanted dynamic loading for any number of reasons ranging from bird impacts to explosions, or shock loading. Therefore, it's imperative that the behavior of these aerospace structures is well understood to ensure the safety of vehicles in some of the most extreme operating conditions. Many critical components in aerospace engines such as turbine blades can be simplified as a thin, cantilever beam. Also, the dynamic loadings experienced by such structures are rarely perpendicular to the surface of the structure, especially keeping in mind the curved or complex geometries involved. Therefore, the current study seeks to understand the structural behavior of cantilevered Hastelloy X plates subjected to extreme temperatures and oblique shock loading. Some amount of research has been done subjecting cantilever plates or beams to dynamic loading. In particular, [2] work on cantilever specimens subjected to tip impact where it was concluded that plastic deformation is concentrated at certain points known as hinges. Also, [3,4] subjected cantilevered specimens to blast loadings using analytical solutions to validate results. However, the amount of work subjecting cantilevers to oblique, dynamic loads is small. Others [5-7] subjected cantilever beams to oblique impacts at the tip. Although none of the aforementioned work has used the material in

question, Hastelloy X. Numerous studies have been done on Hastelloy X, especially at high temperature [12-17 tensile]. Kondo et. al [18] performed impact experiments on Hastelloy X specimens subjected to high temperature helium environments. Abotula et al. [19] developed a constitutive model for Hastelloy X at high temperatures under varying strain rates and found that the material experiences a decrease in yield strength up to 700°C followed by an increase up to 900°C before continuing to decrease. Abotula et al. [20] subjected simply-supported, high temperature Hastelloy X plates to shock loading. The most relevant and the inspiration for this work is Chennametty et. al [21] who subjected clamped-clamped Hastelloy X specimens to shock loading and high temperature. Here, it was found that the angle of incidence governed the amount of plastic deformation and magnitude of deformation. Although much work has been done related to the shock loading of Hastelloy X and other work has been done on cantilever beams, no study has addressed the behavior of cantilevered Hastelloy X. This work seeks to fill the aforementioned gap in knowledge by subjecting Hastelloy X plates at extreme temperatures to different angles of shock incidence.

Experimental Procedures

For the following study, three experiments were conducted for each temperature and incident angle to ensure repeatability. First experiments were conducted with a normal shock incidence (flat) with a 3mm gap from the shock tube at temperatures of 25°C, 400°C, and 800°C. These 3mm gap experiments were conducted as they can be compared to research conducted by [21] and [20] but with different boundary conditions. To explore the effect of oblique shock incidence on the structural behavior, angles of 0° (normal), 15°, and 30° were conducted at temperatures of 25°C, 400°C, and 800°C while keeping the center distance constant (15.7mm).

Material and Specimen Geometry

The material selected for the study was Hastelloy X, a Ni-based superalloy known for its high temperature strength and commonly used in aerospace applications. As shown in Figure 1a, 51 mm x 178 mm x 3mm were clamped on one side using two holes at the bottom of the specimen such that 152 mm remained unsupported. As previously noted, and illustrated in Figure 1b, experiments were conducted at a 3mm gap with normal shock incidence and at a constant gap of 15.7 mm throughout three incident angles of 0°, 15°, and 30°.

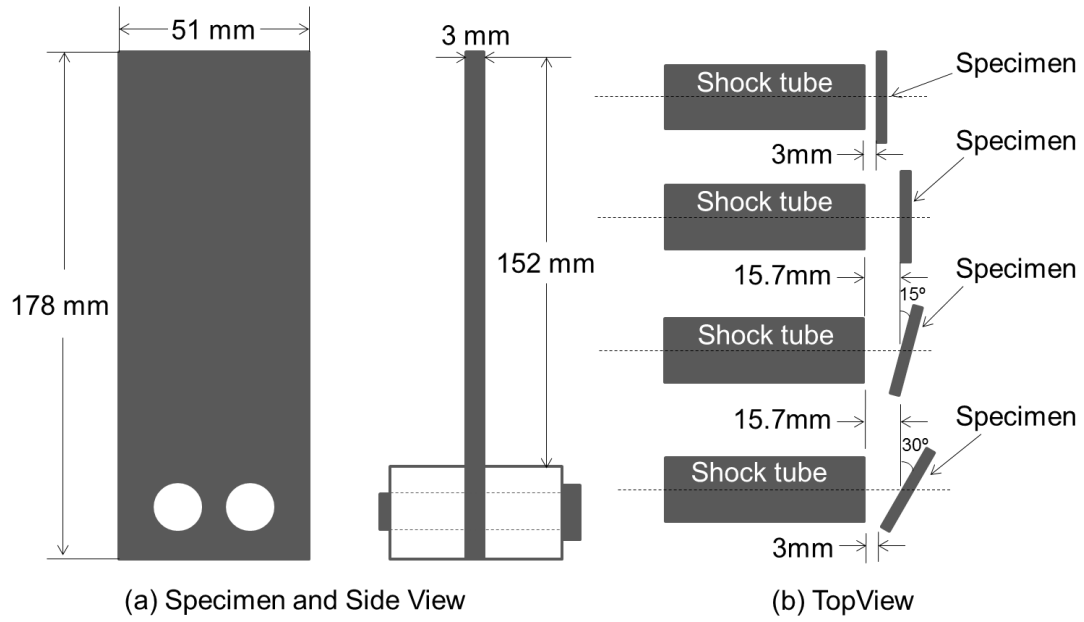

Figure 1: (a) The geometry of the specimen used and a side view of the specimen in the fixture (b) the specimen's orientation relative to the shock tube (top view).

High Temperature

Due to the fact that these structures are subjected to extreme environments during operation, it was necessary to conduct part of this study at high temperatures. However, in order to perform Digital Image Correlation (DIC) and use high speed photography, the application of high temperature had to be non-interfering, non-optically intrusive, and robust to survive multiple shock loadings. Aboutla et al.[16] developed and tested methods using four propane nozzles and proved that this heating method would meet the criteria listed above. The nozzles would be oriented and locked in place such that uniform temperatures could be achieved and temperature gradients could be minimized. The temperature measurements during temperature calibration were obtained using nine Type-K thermocouples whose locations on the specimen are shown in Figure 2a. An example of the data obtained from the thermocouples are shown in Figure 2b. It can be seen that steady-state is reached at

approximately three minutes and a temperature gradient of ±10% of the desired temperature is considered acceptable. Once steady-state temperature is reached, the shock loading can be applied.

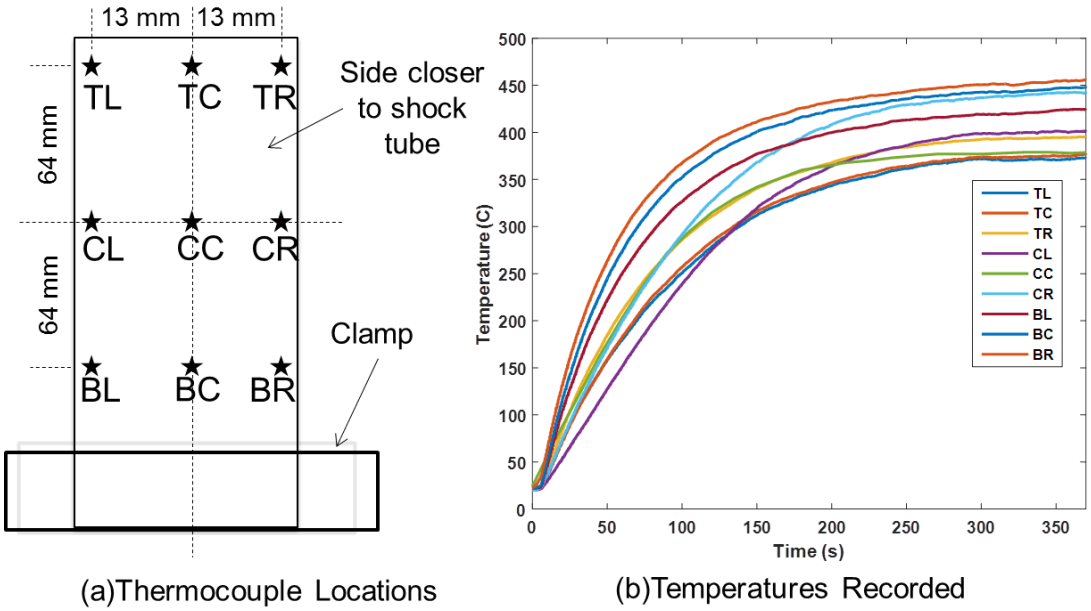

Figure 2: (a) The location of thermocouples on the specimen. (b) A typical plot of temperature vs time for the thermocouple positions in (a).

Shock Tube

Once the specimen was at the desired steady-state temperature, a shock load was applied to the center of the specimen. In order to produce the shock load, a shock tube is used. The shock tube used consists of a driver section, driven section, and a diaphragm which separates the two (Figure 3). The driver section is pressurized until the critical pressure at which the diaphragm ruptures is reached. Once the diaphragm ruptures, the wave travels down the driven section which has an internal geometry such that a shock develops which travels past the pressure sensors at the end of the tube and impinges on the specimen. A typical pressure profile as recorded by the sensors is shown in Figure 4. It can be seen that the first jump by Channel 2 is the

incident pressure, which is typically 0.6 MPa and that the second jump by Channel 1 is the reflected pressure, which is typically 1.7 MPa. This reflected pressure is considered the load applied to the specimen.

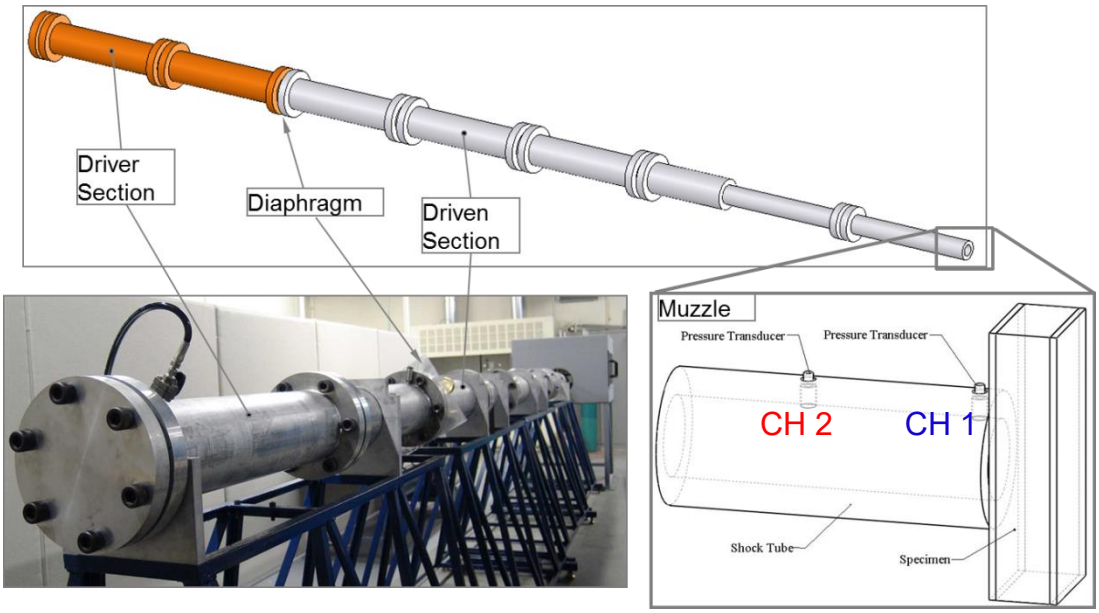

Figure 3: A schematic of the shock tube is shown in the top image supplemented by images of the actual shock tube (bottom left) and a schematic of the muzzle section (bottom right).

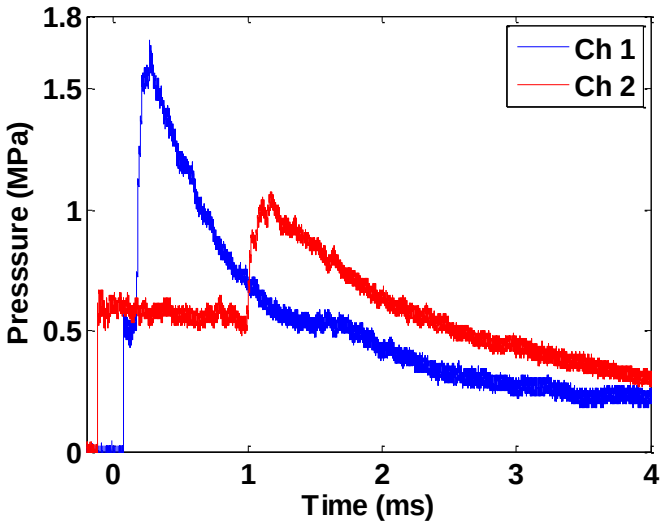

Figure 4: A typical pressure profile captured for a specimen normal and 3mm from the shock tube muzzle.

High Speed Photography and Digital Image Correlation

Due to the extremely dynamic nature of these experiments, the deformation occurs on the order of 10 ms. Therefore, it's imperative that high speed photography is used. For this study, three Photron SA 1.1 cameras were used at frame rates up to 50,000 fps to capture the deformation events. The orientation of the cameras relative to the specimen is shown in Figure 5. One camera was used at the side of the specimen to capture the side-view of deformation. Two cameras at the back face of the specimen were used to obtained stereo images that could be used for 3-D Digital Image Correlation (DIC). However, due to the fact that the specimen would be at extreme temperatures, special techniques were used to obtain images that could be used for DIC. Flame-proof, high temperature paint was used to apply the speckle pattern to the specimen such that high contrast was sustained at extreme temperatures. When the specimen reached high temperatures, the specimen glows red, causing images captured without any filters to be futile due to loss of contrast. Therefore, blue optical bandpass filters were used with a center peak wavelength of 450 nm in conjunction with a high intensity light source (flash) in order to obtain improved images for DIC.

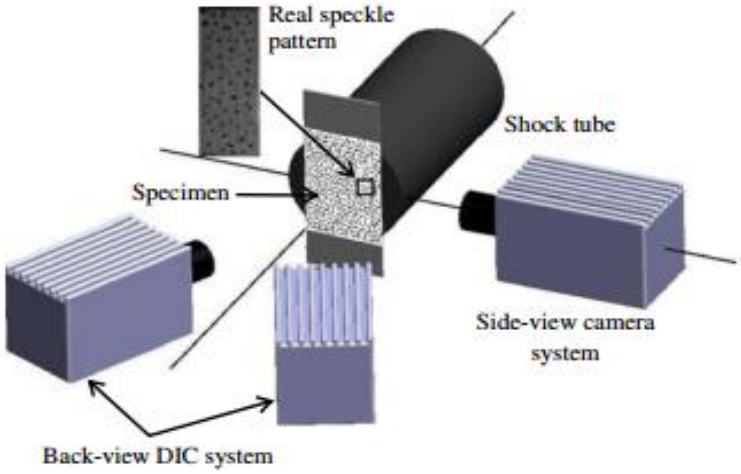

Figure 5: The locations of the cameras in relation to the specimen along with an example of a real speckle pattern used for DIC is shown here.

Results and Discussion

Experiments with a normal angle of shock incidence and a 3mm gap between the specimen and the shock tube muzzle end are discussed first. The following figure (Figure 6) shows the step-wise deformation of a cantilever specimen under shock loading. Figure 6 shows the deflection of the specimen along the center line and Figure 7 shows the corresponding DIC image of out-of-plane deflections. It can be seen that the initial deformation (a) occurs at the center of specimen due to the location of the load. The deformation is symmetric for approximately 1 ms and is predominately elastic. At first, due to the free end, the deflection of the top of the specimen is equal to that of the center (b). However, due to the inertia of the free end, the deflection of the top passes the center and reaches a maximum deflection (c). The maximum deflection is followed by oscillations in which the specimen recovers its elastic deformation (d).

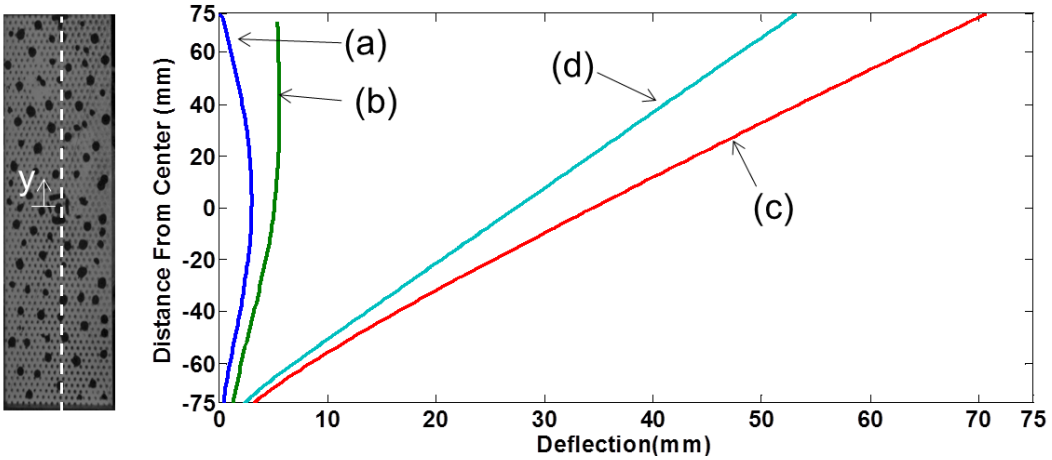

Figure 6: Out-of-plane deflection along the center of the specimen at different time steps.

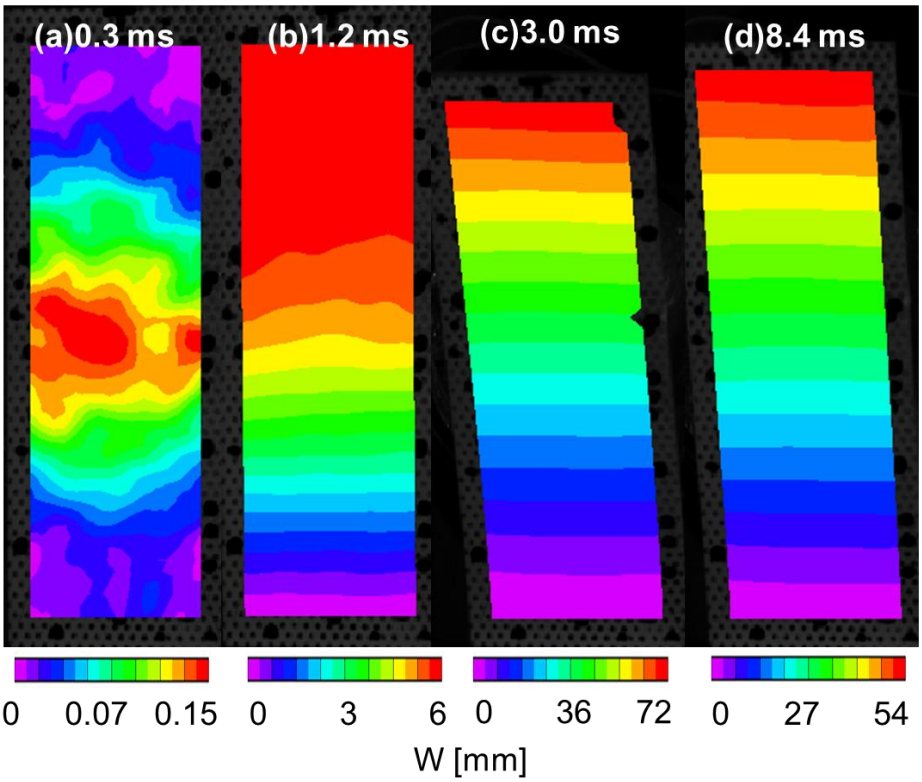

Figure 7: Out-of-plane deflection contours corresponding to the times shown in Figure 6. (The scales of the contours are shown at the bottom of each image.)

For each of the 3mm gap, normal shock experiments, the step-wise deformation is the same for all temperatures. Although the mechanisms of deformation are similar, the magnitude of the out-of-plane deflection changes significantly with increasing temperature. For room temperature, the maximum out-of-plane deflection is about 75 mm. However, at 400°C and 800°C the maximum out-of-plane deflection is about 100 mm and 135 mm, respectively. The out-of-plane deflection at the top of the specimen can be seen in Figure 8. It should also be noted that although the mechanisms of deformation are similar, the difference in magnitude causes the time at which the events described in Figure 6 to be increased as deflection increases. For example, the maximum deflection for the 800°C case occurs at about 11 ms versus about 7 ms for room temperature.

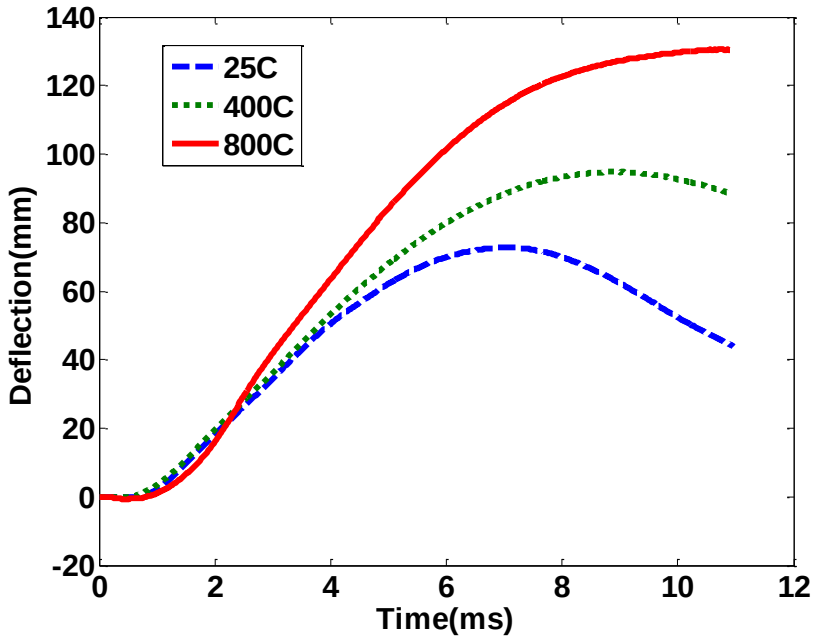

Figure 8: The out-of-plane deflection at the free edge of the specimen as a function of time for three different temperatures.

For the 3mm gap, normal shock experiments, it can be observed that a mode II deformation shape occurs for the case of 800°C. Looking at Figure 9, it can be identified that there is a mode II deformation shape at 800°C, but a mode I deformation shape at 25°C. At 400°C, there is a very subtle curvature at the center of the specimen, indicating a transition region between mode I and mode II. The onset of mode II deformation is caused by the decrease in yield strength as temperature increases. Therefore, when the yield strength reaches a critical value for higher temperatures, the applied load causes local plastic deformation at the center of the specimen in addition to the plastic deformation at the clamped end of the specimen.

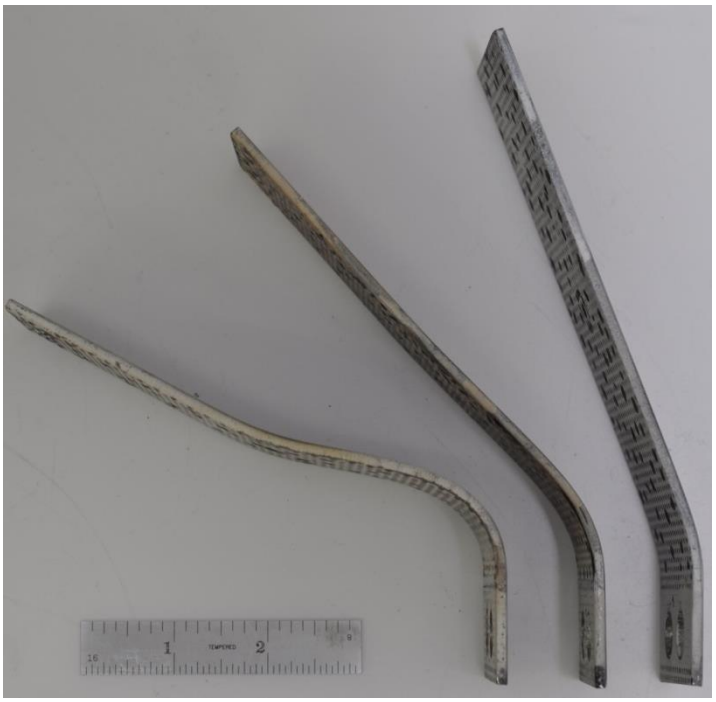

Figure 9: The post-mortem images for 3 different temperatures (from right to left: 800°C, 400°, 25°) for the 3mm gap, normal shock incidence series.

The 15.7 mm gap experiments with normal shock incidence are consistent with the previous series, although as expected, the magnitude of deflection is less as the load applied is less due to the increased distance. For these experiments, mode II deformation is observed although the magnitude of the center deformation of 800°C is lower. Although a typical deformation field looks the same for the normal incident experiment, when the angle is changed to 15° or 30°, the deformation changes. In Figure 10, the out-of-plane deflection for the (a) normal and (b) 30° cases are shown. As seen in (b) at 1.0 ms in the center of the specimen and at 2.4 ms at the free edge, there is a twisting motion of the specimen occurring during the deformation of the 30° specimen. This twisting motion can be seen emerging early in the deformation process at the center of the specimen. As the free edge begins to deflection further than the center, the twisting action is transferred to the free edge. Therefore, as the specimen

deforms out-of-plane, the free edge continues to rotate about the vertical axis of the specimen throughout the deformation.

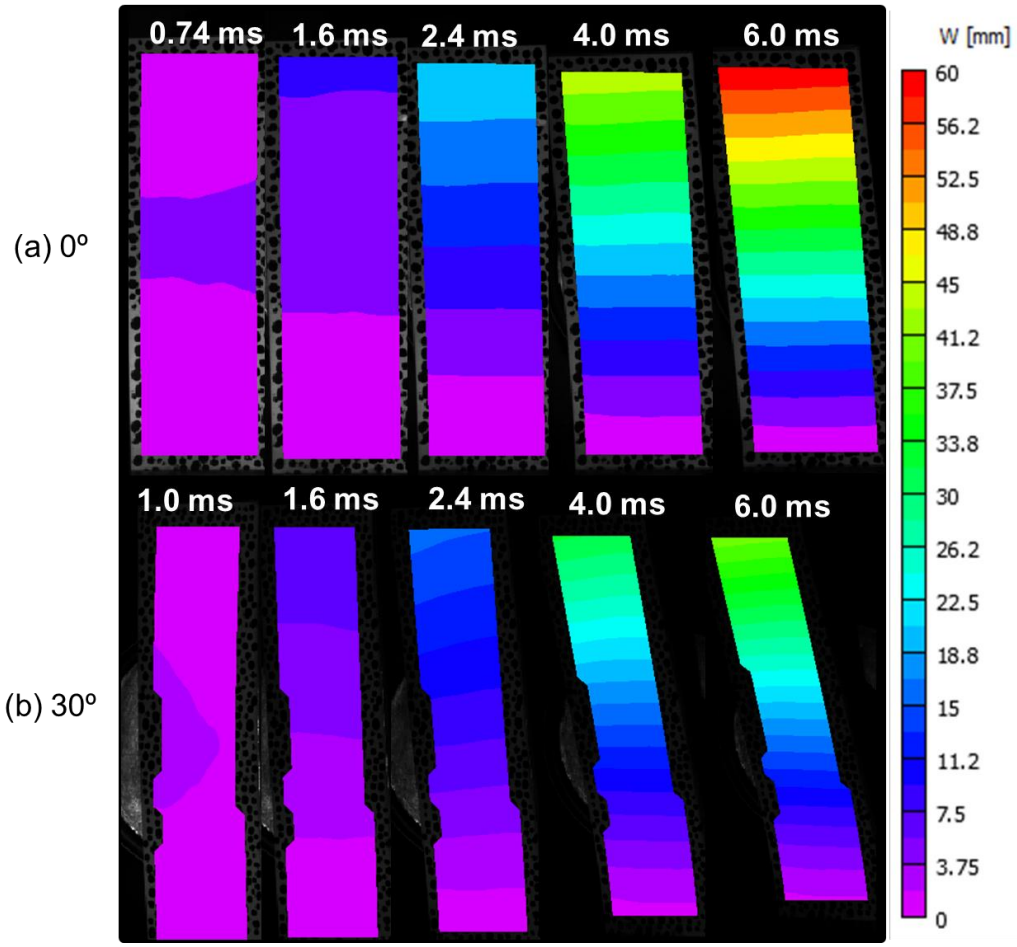

Figure 10: The out-of-plane deflection contours at room temperature for the angles of (a) 0° and (b) 30°.

Therefore, to visualize the twisting action occurring, Figure 11 shows $\varepsilon_{xx,}$ room temperature contours in one millisecond intervals. It can be seen that early in time, at around 1 ms, the light-blue strain contour near the center of the specimen represents an area of twisting. In the other images, it can be seen that the left edge has large purple or blue contours which indicates that twisting continues through 5 ms into the event. Due to the fact that the maximum deflection occurs near this time, it is obvious that the specimen twists throughout the entire deformation event until the maximum

deformation is reached. After the maximum deflection is reached, however, the out-of-plane deformation and twisting both begin to damp and are minimized.

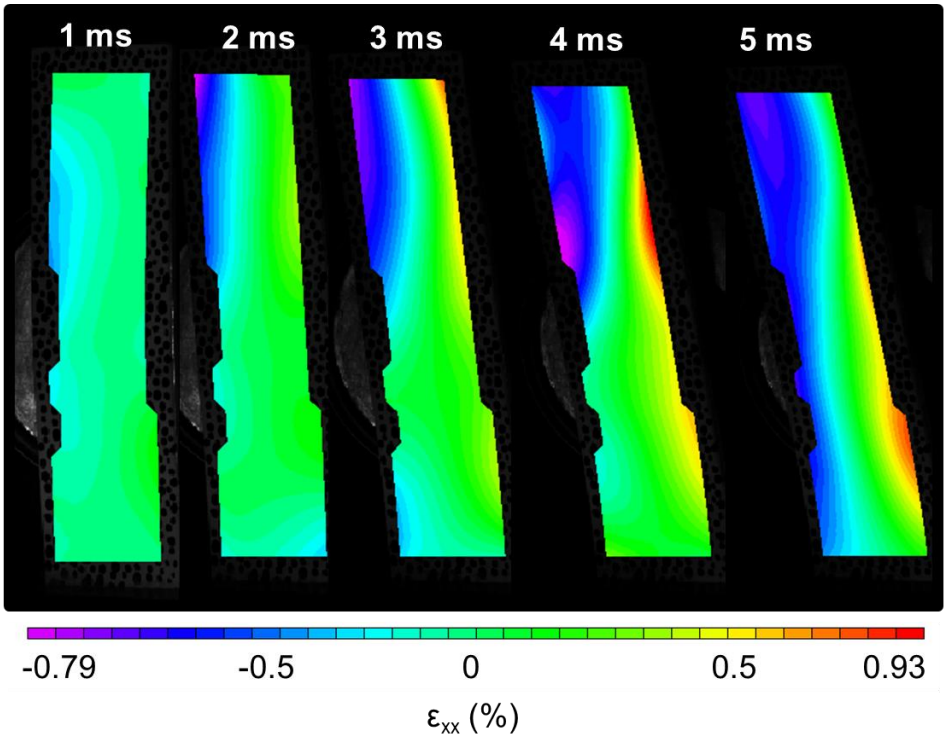

Figure 11: The strain (ε_{xx}) contours for the 30° angle at room temperature.

As previously mentioned, the aim of this work is to study the structural deformation as it pertains to aerospace structures. Therefore, the velocity of the structure at various times during the event is of the utmost importance. Figure 12 compares the velocity of the normal and 30° cases at room temperature. It can be seen that the twisting causes the maximum velocity to oscillate between the left and right edge as opposed to a constant velocity across the width of the free edge.

However, looking at post-mortem DIC images, it can be seen that there is no residual effects of twisting. Therefore, it can be concluded that the twisting action is only an elastic behavior.

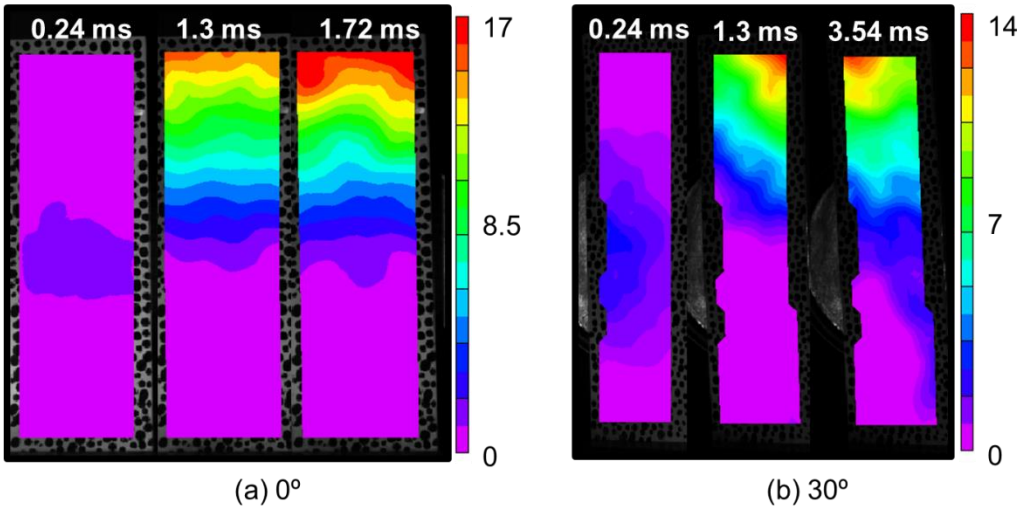

Figure 12: The velocity (m/s) contours for the angles of (a) 0° and (b) 30°.

In Figure 13, the out-of-plane deflection of the free edge of the specimen is shown as a function of time for the three angles in which the center distance was kept constant. It can be seen from Figure 13 that the out-of-plane deflection increases with increasing temperature do to a decrease in yield strength. It is also evident that the out-of-plane deflection decreases with increasing angle. However, even with the center distance constant, the loading scenario is slightly different on each specimen.

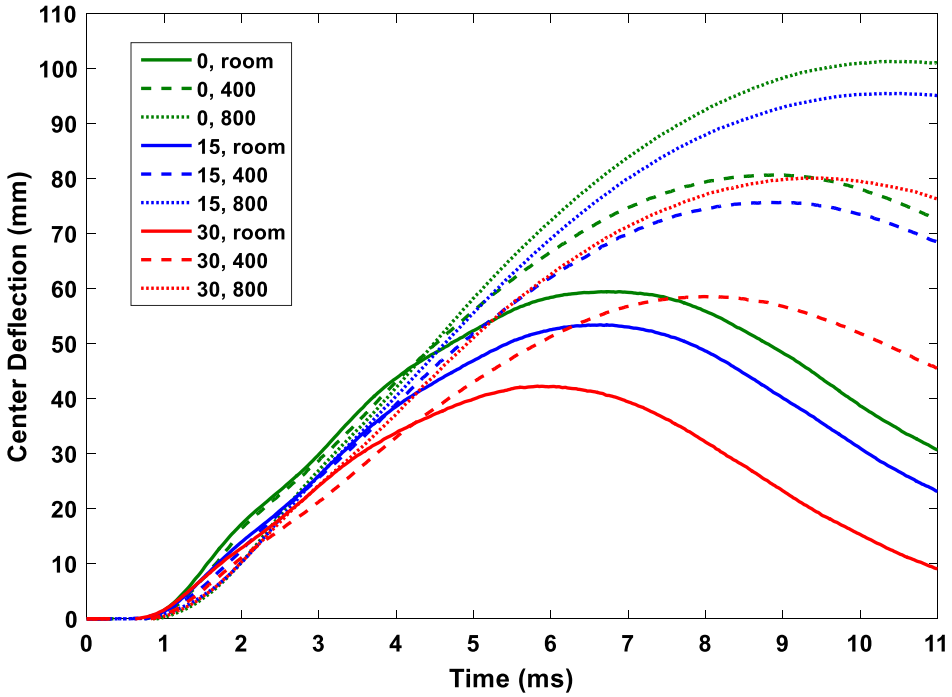

Figure 13: The free edge, out-of-plane displacements as a function of time for each experiment conducted.

For a normal shock incidence and small gap between the specimen and the shock tube, the reflected pressure obtained by Channel 1 in the shock tube has been proven to closely depict the pressure *felt* by the specimen. However, due to the fact that the shock is free to expand, as the distance is increased, or the angle is not normal to muzzle, the pressure obtained by the sensors on the muzzle do not necessarily reflect the pressure that impinges on the specimen. Typically, an incident pressure of 0.6 MPa causes a reflected pressure of 1.7 MPa due to the compressibility of air which causes a spring-like effect. However, specimens that are not normal to the muzzle do not experience the same spring-like effect and, therefore, the pressure felt by the specimen cannot be assumed. Therefore, three pressure sensors were out-fitted to rigid plates across the 51 mm width. By setting up these plates at the same orientation the

experiment would be conducted, pressure data could be obtained on the surface of the specimen. When normalizing magnitude of deformation for different oblique instances, it is found that there is not significantly different.

Conclusions

A comprehensive series of experiments were conducted subjecting cantilevered Hastelloy X plates to extreme temperatures and oblique shock loading. Experiments were conducted at temperatures of 25°C, 400°C, and 800°C and shock angles of 0° (normal), 15°, and 30° while keeping the center of the specimen a constant 15.7mm away and one 0° series of temperatures as conducted with the specimen closer to the shock tube (3mm). A high speed optical arrangement capable of obtaining Digital Image Correlation data was used to develop an understanding of the material's structural behavior in such loading conditions. Through these experiments, the following major conclusions were made:

- There is a step-wise deformation of a cantilever beam under dynamic loading where the specimen begins to deform symmetrically but asymmetry occurs due to the inertia of the free edge.
- The out-of-plane deflection increases with temperature for all incident shock angles.
- As temperature increases, a mode II deformation shape becomes more visible. The closer the specimen is to the muzzle of the shock tube, the more prominent the mode II deformation shape is.
- A twisting phenomenon occurs when the incident shock is oblique. However, there is no residual twisting in the

structure and, therefore, the twisting is strictly an elastic behavior.

- When normalized with load, there is no difference in the deformation when comparing different shock incident angles.

Acknowledgements

The authors would like to thank Air Force Office of Scientific Research (AFOSR) under Grant No. FA9550-13-1-0037. The authors would also like to thank their colleagues in the Dynamics Photo-Mechanics Laboratory.

References

[1] Spittle, P., (2003). Gas turbine technology, *Physics Education*, 38(6):504-511.

[2] Parkes, E.W., (1955). The permanent deformation of a cantilever struck transversely at its tip. *Proc. R. Soc. Lond*. A228:462-476.

[3] Librescu, L., & Na, S. S., (1998). Dynamic response of cantilevered thin-walled beams to blast and sonic-boom loadings. *Shock. Vib., 5*(1):23–33.

[4] Hall, R.G., Al-Hassani, S.T.S., Johnson, W., (1971). The impulsive loading of cantilevers.*Int. J. Mech. Sci*. 13:415–430.

[5] Shu, D., Stronge, W. J., & Yu, T. X. (1992). Oblique impact at the tip of a cantilever. *Int. J. Impact Engineering.* 12(1): 307–47.

[6] Rao, S.S., Raghavan, K.S., (1987). Dynamic inelastic response of beams and plates under combined loading. *J. Appl. Mech*. 54: 228-230.

[7] Yu, T.X. (1991). An analytical model of the cantilever beam subjected to oblique impact. *Sci China.* 34: 191-200.

[8] Swaminathan, B., Abuzaid, W., Sehitoglu, H., & Lambros, J. (2014). Investigation using digital image correlation of Portevin-Le Chatelier in Hastelloy X under thermo-mechanical loading. *International Journal of Plasticity*, *64*, 177–192.

[9] Sakthivel, T., Laha, K., Nandagopal, M., Chandravathi, K. S., Parameswaran, P., Panneer Selvi, S., Mannan, S. K. (2012). Effect of temperature and strain rate on serrated flow behaviour of Hastelloy X. *Materials Science and Engineering A*, *534*, 580–587.

[10] Aghaie-Khafri, M., & Golarzi, N. (2008). Forming behavior and workability of Hastelloy X superalloy during hot deformation. *Materials Science and Engineering: A*, *486*(1-2), 641–647.

[11] Lai, G. Y. (1978). An investigation of the thermal stability of a commercial Ni-Cr-Fe-Mo alloy (hastelloy alloy X). *Metallurgical Transactions A*, *9*(6), 827–833.

[12] Rowley M.A., Thornton E.A., (1996). Constitutive modeling of the visco-plastic reponse of Hastelloy-X and Aluminium alloy 8009. *Journal of Engineering Materials and Technology*, 118:19–27 [11]

[13] Kim, W. G., Yin, S. N., Ryu, W. S., Chang, J. H., & Kim, S. J. (2008). Tension and creep design stresses of the “Hastelloy-X” alloy for high-temperature gas cooled reactors. *Materials Science and Engineering A*, *483-484*(1-2 C), 495–497.

[14] Kondo, Y., Fukaya, K., Kunitomi, K., & Miyamoto, Y. (1988). Tensile and impact properties changes of HASTELLOY X after exposure in high-temperature helium environment. *Metallurgical Transactions A*, *19*(5), 1269–1275.

[15] Abotula S., Shukla A., Chona R., (2011). Dynamic constitutive behavior of Hastelloy X under thermo-mechanical loads, *Journal of Material Science*, 46(14):4971–4979.

[16] Abotula, S., Heeder, N., Chona, R., & Shukla, A. (2013). Dynamic Thermo-mechanical Response of Hastelloy X to Shock Wave Loading. *Experimental Mechanics*, *54*(2), 279–291.

[17] Chennamsetty, A. R. K., LeBlanc, J., Abotula, S., Naik Parrikar, P., & Shukla, A. (2015). Dynamic response of Hastelloy® X plates under oblique shocks: Experimental and numerical studies. International *Journal of Impact Engineering*, *85*, 97–109.

Conclusions & Future Work

Two comprehensive studies were completed subjecting superalloy Hastelloy X plates to extreme environments with the intent of understanding the structural behavior of aerospace structures under high temperature and shock loading. These studies were completed using unique facilities and equipment including but not limited to a shock tube and high speed cameras at the University of Rhode Island. One study subjected high temperature, pre-loaded specimens to normal shock loading while another study subjected high temperature, cantilever specimens to oblique shock loadings. Through these studies, a better understanding of the underlying physics during the deformation of Hastelloy X plates was established. Specifically, it was observed that for both boundary conditions, a change in deformation mode appears as temperature increases.

To further develop an understanding the structural behavior of the material, more studies should be conducted. Currently, work has only been done on high temperature, pre-loaded plates for normal shock loading. Changing the angle of the incident shock would cause a different indentation shape which would be interesting to study. Also, in the case of the cantilever specimen, increasing the pressure to create a plastic twisting phenomenon would be significant. Also, for all of the cases mentioned, it would be important to know the dominant mechanisms as the shock pressure continues to increase. It is of critical importance to understand the structural behavior of these aerospace components under a myriad of different shock conditions.

The work presented here focuses on a single geometry. However, combustion end components could be a variety of geometries. Even when only considering turbine blades, the length and width can vary depending on the engine in

consideration. Also, some combustion end components, especially turbine blades, have some sort of curvature to them. If this study could be extended to combustion end components of various lengths, widths, or curvatures, it would be very helpful to the aerospace industry. Here, it may be best to develop a simulation which can be confirmed with the results shown and extended to any number of geometries.

All of this work has only considered Hastelloy X, which, although this material is one of the most widely used nickel-based superalloys, it is important that other nickel-based superalloys in use are well understood. Similar experiments to those discussed in this work can be run with different nickel-based superalloys to have confidence in the structural behavior of all aerospace materials.